

AD-A094 736

AIR FORCE INST OF TECH WRIGHT-PATTERSON AFB OH SCHOO--ETC F/8 14/2
A PARAMETRIC STUDY OF CERTAIN FORCING FUNCTIONS RELATED TO A HY--ETC(U)
DEC 80 V A TISCHLER
AFIT/6AE/AA/80D-22

UNCLASSIFIED

NL

1 OF 1
AD
A094736

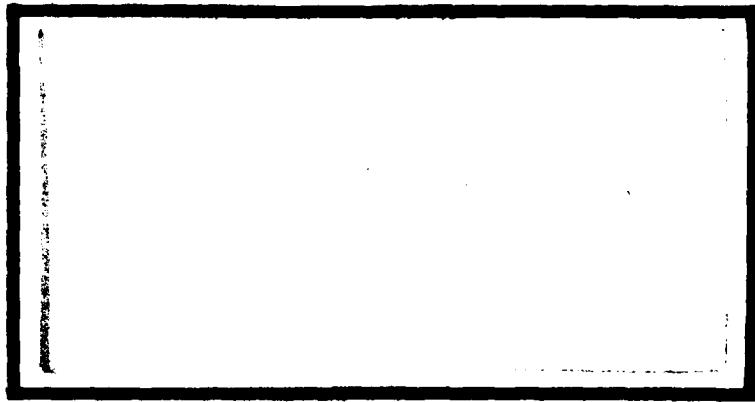
END
DATE
FILMED
3 81
DTIC

AD A094736



LEVEL

①



DTIC
SELECTED
FEB 9 1981

DDC FILE COPY

DEPARTMENT OF THE AIR FORCE
AIR UNIVERSITY (ATC)
AIR FORCE INSTITUTE OF TECHNOLOGY

Wright-Patterson Air Force Base, Ohio

DISTRIBUTION STATEMENT A
Approved for public release;
Distribution Unlimited

81 2 09 024

23 JAN 1981

APPROVED FOR PUBLIC RELEASE AFR 190-17.

Laurel A. Lampela
LAUREL A. LAMPELA, 2Lt, USAF
Deputy Director, Public Affairs

Air Force Institute of Technology (ATC)
Wright-Patterson AFB, OH 45433

RECEIVED
JAN 9 1981

A PARAMETRIC STUDY OF CERTAIN FORCING FUNCTIONS
RELATED TO A HYPERSONIC SLED

THESIS

AFIT/GAE/AA/80D-22 Victoria A. Tischler

Approved for public release; distribution unlimited.

A PARAMETRIC STUDY OF CERTAIN FORCING FUNCTIONS
RELATED TO A HYPERSONIC SLED

7 12
THESIS

Presented to the Faculty of the School of Engineering
of the Air Force Institute of Technology
Air University
in Partial Fulfillment of the
Requirements for the Degree of
Master of Science

by
Victoria A./Tischler
Graduate Aeronautical Engineering

11 December 1980

Approved for public release; distribution unlimited.

PREFACE

The interest of this thesis is the dynamics of rocket sleds traveling on rails at supersonic and hypersonic speeds. The analytical model chosen for simulating the dynamics of a sled ride consists of three subsystems: (1) the elastic sled body, (2) the slipper beam (springs), (3) and the rail roughness profile. A parametric study involving a variation of the rail roughness profile and the slipper stiffnesses was conducted.

I am grateful to my thesis advisor, Dr. Anthony Palazotto, for his valuable advice and direction given throughout this project. I am also grateful to Dr. Vipperla Venkayya, my thesis committee member, for critically reviewing this thesis. A special thanks to Ms. D. Frantz for her patience and understanding while typing this thesis.

Victoria A. Tischler

Accession For	
NTIS GRI&I	<input checked="checked" type="checkbox"/>
DTIC TAB	<input type="checkbox"/>
Unannounced	<input type="checkbox"/>
Justification	
By _____	
Distribution/	
Availability Codes	
Dist	Avail and/or Special
A	

CONTENTS

	<u>Page</u>
Preface	ii
List of Figures	iv
List of Tables	v
Symbols	vi
Abstract	ix
I. Introduction	1
II. Development of the Simulation Equations	8
III. Description of an Integrated Design Tool	22
IV. Simulation of Rail Roughness Profiles	26
V. Results	34
VI. Conclusions	54
References	57
Appendix A: Derivation of Damping Coefficients	59
Vita	64

List of Figures

<u>Figure</u>	<u>Page</u>
1. Ten Mile Test Track at Holloman AFB	2
2. Sled Train	3
3. Rocket Sled Slipper and Test Track Cross-Section	4
4. Integrated Design Tool	23
5. Sled Geometry	24
6. SLEDYNE Rail Roughness Profile for the Right Rail	28
7. Monte Carlo Rail Roughness Profile for the Right Forward Slipper	33
8. General Arrangement - MX Forebody Configuration A	35
9. Finite Element Model of the MX Forebody Configuration A	36
10. The First Six Frequencies and Mode Shapes	43-44
11. Deformation Plots - Original SLEDYNE Profile $k_A=k_F=48.0 \times 10^4$.	48
12. Deformation Plots - Original SLEDYNE Profile $k_A=k_F=96.0 \times 10^4$.	49
13. Deformation Plots - Original SLEDYNE Profile $k_A=k_F=192.0 \times 10^4$.	50
14. Deformation Plots - Monte Carlo Profile $k_A=k_F=48.0 \times 10^4$. . .	51
15. Deformation Plots - Monte Carlo Profile $k_A=k_F=96.0 \times 10^4$. . .	52
16. Deformation Plots - Monte Carlo Profile $k_A=k_F=192.0 \times 10^4$. . .	53

List of Tables

<u>Table</u>		<u>Page</u>
1.	Probability Distribution of Rail Roughness	30
2a.	Maximum Accelerations in $\text{in/sec}^2/10^5$ - Original SLEDYNE Profile	45
2b.	Maximum Accelerations in $\text{in/sec}^2/10^5$ - Monte Carlo Profile	46
3a.	Total Strain Energy of the Sled in in/lb - Original SLEDYNE Profile	47
3b.	Total Strain Energy of the Sled in in/lb - Monte Carlo Profile	47

List of Symbols

$[C]$	damping matrix
C_A	damping coefficient for the aft slippers
C_b	damping coefficient at each slipper for bounce
CDF	cumulative distribution function
C_F	damping coefficient for the forward slippers
C_P	damping coefficient at each slipper for pitch
D_A	damping forces at the aft slippers
D_F	damping forces at the forward slippers
$f(x_j)$	probability that x_j occurred in the j th interval
$\{F\}$	vector of input forces
$\{F_I\}$	vector of inertial forces
F_A	aft slipper force
F_{A_s}	aft spring force
F_F	forward slipper force
F_{F_s}	forward spring force
F_S	quasi-steady forces
F	Rayleigh's dissipation function
$FREQ_j$	the number of rail measurements occurring in the j th interval of Table 1
I	pitch inertia of the sled
$[k]$	stiffness matrix of the sled
$[K]$	generalized stiffness matrix
k	number of modes included in the simulation equations
k_A	aft slipper support stiffness
k_F	forward slipper support stiffness
l	distance between the forward and aft slipper

l_A	distance from the sled cg to the aft slippers
l_F	distance from the sled cg to the forward slippers
$[m]$	diagonal matrix of the lumped parameter system
m_{ii}	lumped mass at the i th node
$[M]$	generalized mass matrix
m	total mass of the sled
M_s	quasi-steady moment
N	number of nodes of the finite element model
$P(a=b)$	probability that $a=b$
$q_i(t)$	normal coordinate or amplitude of $\{\phi(x)\}_i$
Q_i	i th nonconservative force
$RANF(A)$	random number generator function
t	time in secs
T	kinetic energy
t_f	total time of the sled run in secs
$\{u\}$	vector of displacements corresponding to the number of degrees of freedom of the sled
U	strain energy
v	sled downtrack velocity
$\{V_i\}$	set of 430 measurements of rail height
VAL_j	value assigned to the j th interval of Table 1
$w(x,t)$	vertical displacement of the sled at time t and station x along its horizontal axis
W	work done by the slipper springs on the rigid displacements
x	position of the sled along its horizontal axis
x_{cg}	position of the center of gravity of the sled along its horizontal axis
\bar{X}_T	total distance that the sled will travel
\underline{XX}	random variable

$Y(\bar{X})$	rail height when the aft slippers are at downtrack position \bar{X}
$Y(\bar{X}+l)$	rail height when the forward slippers are at downtrack position $(\bar{X}+l)$
$z(t)$	vertical translation at time t
γ	proportionality constant
θ	rotation of the sled about its center of gravity
ϵ	slipper gap in in.
ξ_i	proportion of critical damping for the i th mode
ξ_θ	proportion of critical damping for pitch
ξ_z	proportion of critical damping for bounce
$\{\eta\}$	vector of the independent variables of motion
λ_i	frequency in hz of the i th normal mode
$\{\phi\}_i$	i th normal mode of vibration
ϕ_{ji}	j th component of the i th mode
ω_i	natural frequency of the i th normal mode

ABSTRACT

→ The rail roughness profile and the slipper stiffnesses are the important factors in determining the forcing function in the dynamic analysis of high speed rocket sleds. A parametric study involving a variation in the rail roughness profile and the slipper stiffnesses was performed. This study was carried out by interfacing the NASTRAN structural analysis program and a program called SLEDYNE developed for Holloman AFB. Using NASTRAN a free vibration analysis of the elastic sled body was made in order to obtain the natural frequencies and mode shapes. SLEDYNE simulates the sled ride on the rails and computes a set of inertial forces acting on all the mass points of the sled. The response of the sled to this inertial loading was determined by a NASTRAN static analysis.

Two rail roughness profiles were considered, both based on the same set of track measurements, and three values of slipper stiffness were used. Response to the parametric study was measured by the total strain energy of the sled and the displacements of the mass points of the sled. ↗

A PARAMETRIC STUDY OF CERTAIN FORCING FUNCTIONS
RELATED TO A HYPERSONIC SLED

I. INTRODUCTION

For a number of years both the Air Force and the Navy have been using high speed sleds on a test track to simulate the dynamic environment of flight vehicles. A ten mile test track, Fig. 1 has been operated by the Air Force at Holloman AFB for a number of years.⁽¹⁾ Test sleds that are capable of attaining speeds up to Mach 6 have been built to test the crew escape systems, the effects of rain or particle erosion on re-entry vehicles, missile guidance systems etc. Most of these sleds consist of a forebody to house the test objects and a rocket train acting as a pusher, Fig. 2. There are dual rail as well as monorail sleds. The riding mechanism consists of a set of fore and aft slippers attached to the sled and capable of riding on the rails as shown in Fig. 3.⁽²⁾ An 1/8" gap between the rails and the slippers is usually incorporated. During the ride the slipper may be in any of the following three positions: (a) in contact with the top of the railhead, (b) in contact with the underside of the railhead or (c) no contact at all. From an analysis standpoint it becomes necessary to appreciate the rail roughness and the external aerodynamic forces which induce pitch and bounce motion during the ride. This motion in turn induces high inertia forces on the sled. Accurate determination of these inertia forces requires extensive dynamic analysis and testing.

Research in the dynamic analysis and simulation of vehicles traversing on rough terrain has been drawing increasing attention in recent years. The problem is of generic interest to a number of organizations. For example, the automotive industry is interested in this problem in order to



Figure 1. Ten Mile Test Track at Holloman AFB

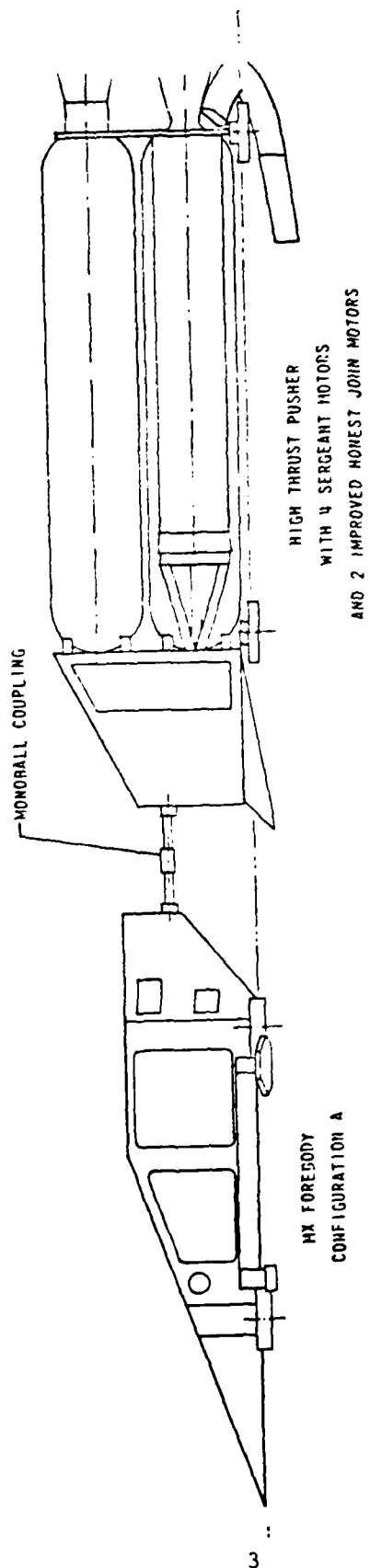


Figure 2. Side View of the Sled Train

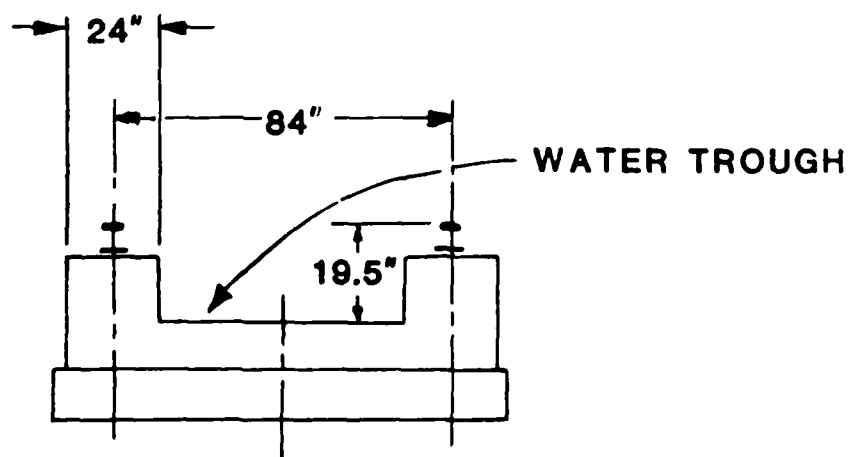
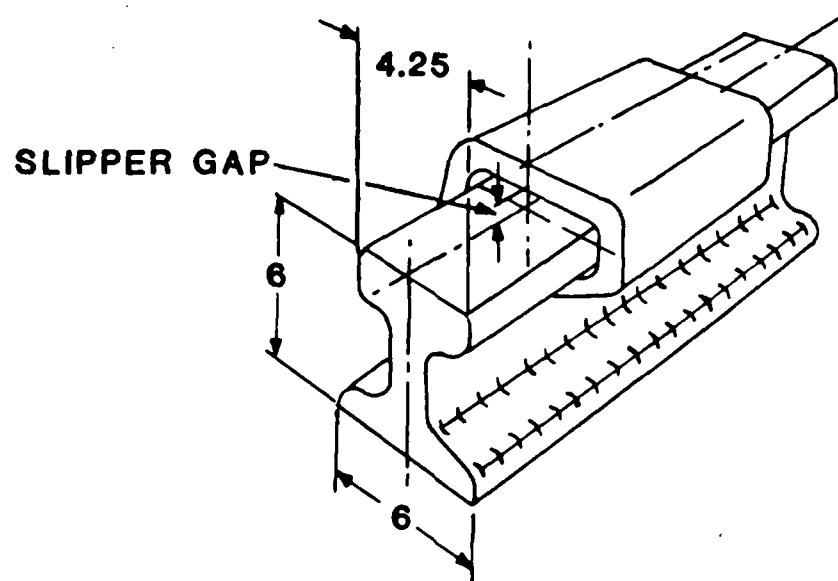


Figure 3. Rocket Sled Slipper and Test Track Cross-section

gain a competitive edge by improving the ride quality of their vehicles. The safety and structural integrity of airplanes taking off from bomb damaged runways is of the utmost concern to the Air Force. Under the "HAVE BOUNCE" program the Air Force is developing runway repair standards for a number of airplanes in its inventory.⁽³⁾ Similar problems are encountered by Army vehicles while traveling on unpaved terrains. The interest of the present study is the dynamics of test sleds traveling on rails at supersonic and hypersonic speeds.

The analytical model for simulating the dynamics of a vehicle ride generally consists of four subsystems:⁽⁴⁾ (1) the vehicle body, (2) a suspension system, (3) tires and (4) terrain. The speed of the vehicle, the surrounding environment and the terrain profile provide the dynamic input to the system, while the stiffness, mass and damping properties of the remaining three subsystems determine the dynamic response. The environment and the terrain profile are generally described by random parameters. Even though the stiffness, mass and damping properties are deterministic, they cannot be accurately represented by analytical models because of their complexity. The usual procedure is to represent the subsystems by simple empirical models and validate the empirical parameters by extensive testing.

Improving the numerical modeling of the subsystems is the current research interest in vehicle system dynamics. The models can range from very simple linear models to complex nonlinear representations. An interesting discussion on tire models for dynamic vehicle simulation is presented in Ref. 4. Four tire models were considered, and each model was integrated with the other three subsystems to simulate a complete terrain-vehicle model to study the dynamic tire behavior. The paper contains

analytical and experimental results obtained from a three axle military truck. A computer program to analytically simulate the rough ride on bomb damage runways was developed by the Boeing Company for the Air Force.⁽³⁾ The mathematical model of the aircraft includes horizontal, vertical and pitch rigid body modes, elastic modes of the airframe, and nose and main landing gear modes. Tire forces are generated by a nonlinear spring model. The program is quite preliminary, and it is being tested for validation.

A computer program called "SLEDYNE" for simulating a sled ride on rails was developed for Holloman Air Force Base.⁽⁵⁾ The elastic sled body, slipper beams (springs) and rail roughness profile are the subsystems considered in the program. The flexible modes of the body and the necessary mass matrices are generated external to the SLEDYNE program. The basis for the rail roughness profile is measured data from 400 feet of track. This data is used as a random sample to generate the profile for the entire length of the track. The slipper-rail stiffness parameters are empirical and are input to the program. Similarly the aerodynamic parameters are the external input. The mathematical model includes two rigid body modes (the bounce and the pitch) and a number of elastic modes of the body. The intermittent contact between the slippers and the rails induce discontinuous force input. The transient response of the vehicle is determined by numerical integration of the dynamic equations. The peak accelerations, velocities, displacements and the inertia forces at all the mass points are the measures of the response.

The SLEDYNE program represents a preliminary attempt at generating a rational dynamic model for simulating a high speed sled ride on rails, but the documentation of the program is less than adequate. There are practically no guidelines as to how the slipper-rail stiffness parameters are to

be generated or how they affect the response. Similar deficiencies abound in the description of the aerodynamic and other empirical parameters.

The purpose of this effort is to study the potential and limitations of the SLEDYNE program, expand its documentation and make parametric studies with the slipper-rail stiffnesses and rail roughness profile.

II. DEVELOPMENT OF THE SIMULATION EQUATIONS

The movement of a vehicle along a rail bed would obviously induce high inertia forces which in turn produce severe dynamic stresses and displacements. The dynamic stresses required for predicting the sled's strength, with adequate margins of safety, can be obtained by a dynamic analysis using a finite element model of the sled. However, the transient response analysis of the full model can be prohibitively expensive and thus is not very conducive to design trade studies. Yet, it is possible to study a reduced system of equations for the transient response by modal reduction. The significant modes (i.e. the primary bending modes) that participate in the pitch and bounce motion are determined by a free vibration analysis of the full finite element model of the sled with supports at the slippers. The dynamic reduction is carried out by combining a few elastic bending modes with two rigid body modes which can adequately simulate the dynamic motion of the sled. In order to generate the dynamic forces for analysis, the use of SLEDYNE with the NASTRAN program was carried out as subsequently discussed. Yet to supplement the readers understanding of SLEDYNE's analytic approach to the dynamic equations, the author will present the necessary expressions and their development so that the effect of changes in rail roughness and slipper stiffness can be more fully appreciated.

A finite element model of a sled consists of a number of nodes connected by elements. Each node is assumed to have six degrees of freedom (three translations and three rotations). The dynamic equations for free vibration of a sled can be written as

$$[m]\{\ddot{u}\} + [k]\{u\} = 0 \quad (1)$$

where $\{u\}$ is a vector of displacements corresponding to the number of degrees of freedom of the sled, and $[m]$ is the diagonal matrix of the lumped parameter system such that m_{ii} is the lumped mass at the i th node, and $[k]$ is the sled's stiffness matrix.

The solution of the harmonic equation is given by

$$\begin{aligned}\{u\} &= \{\phi\} \cos (\omega t + \psi) \\ \{\dot{u}\} &= -\omega \{\phi\} \sin (\omega t + \psi) \\ \{\ddot{u}\} &= -\omega^2 \{\phi\} \cos (\omega t + \psi)\end{aligned}\tag{2}$$

Substituting Eq. (2) into Eq. (1) gives

$$(-\omega^2 [m] \{\phi\} + [k] \{\phi\}) \cos (\omega t + \psi) = 0$$

which implies

$$\omega^2 [m] \{\phi\} = [k] \{\phi\}\tag{3}$$

Eq. (3) represents a standard eigenvalue problem. Its solution gives the eigenvalues and eigenvectors which represent the frequencies and mode shapes, respectively. Thus $\{\phi\}_i$ is the normal mode of vibration associated with frequency ω_i .

By providing supports at the slippers, only the motion due to deformation of the sled is considered in Eq. (1). This motion must be enhanced to include rigid body modes for a true representation of the sled ride. This enhancement as well as the reduction in the system of equations can be accomplished by representing the motion of the sled in the vertical direction, w , as the sum of a set of displacement functions: the pure vertical translation, z , the rotation, θ , of the rigid sled about its center of gravity (cg), and the normal modes of vibration, $\{\phi\}_i$, of the sled restrained against translation at the slipper support points. The $\{\phi\}_i$ are orthogonal to each other but not to the rigid body functions. Therefore the vertical displacement, w , of a sled, at time t and station x

along its horizontal axis is given by

$$w(x,t) = z(t) + (x-x_{cg})\theta(t) + \sum_1 \{\phi(x)\}_1 q_1(t) \quad (4)$$

where $q_1(t)$ is the normal coordinate or amplitude of $\{\phi(x)\}_1$. The first few transverse bending (vertical) modes are included in this representation. The $\{\phi(x)\}_1$ in Eq. (4) contain only the vertical components.

Since the structure of the sled has been idealized as a finite element model, the vertical motion of the discrete node points on the sled is given by

$$\begin{Bmatrix} w_1(x,t) \\ \vdots \\ w_N(x,t) \end{Bmatrix} = \begin{Bmatrix} 1.0 \\ \vdots \\ 1.0 \end{Bmatrix} z(t) + \begin{Bmatrix} x_1 - x_{cg} \\ \vdots \\ x_N - x_{cg} \end{Bmatrix} \theta(t) + \begin{bmatrix} \phi_{11} & \phi_{12} & \dots & -\phi_{1k} \\ \phi_{21} & \phi_{22} & \dots & -\phi_{2k} \\ \vdots & \vdots & \ddots & \vdots \\ \phi_{N1} & \phi_{N2} & \dots & -\phi_{Nk} \end{bmatrix} \begin{Bmatrix} q_1(t) \\ \vdots \\ q_k(t) \end{Bmatrix} \quad (5)$$

where N is the number of nodes of the original finite element model, k is the number of modes included such that $0 \leq k \leq N$, and $\phi_{ij}(x)$ is the i th component of the j th mode.

The equations of motion will be derived using Lagrange's equation⁽⁶⁾

$$\frac{d}{dt} \left(\frac{\partial T}{\partial \dot{\eta}_i} \right) + \frac{\partial U}{\partial \eta_i} + \frac{\partial F}{\partial \eta_i} = \frac{\partial W}{\partial \eta_i} + Q_i \quad (6)$$

where T is the kinetic energy, U is the strain energy, F is Rayleigh's dissipation function, W is the work and Q_i are the nonconservative forces. The η_i represent the independent variables of motion, z , θ , and q_j , $j=1, \dots, k$.

The kinetic energy T is given by

$$T = \frac{1}{2} \{\dot{w}\}^T [m] \{\dot{w}\} \quad (7)$$

The mass matrix $[m]$ contains only the degrees of freedom corresponding to the vertical displacements of the nodes.

Substituting Eq. (5) into Eq. (7) gives

$$T = \frac{1}{2} \left\{ \begin{bmatrix} \{1.0, \dots, 1.0\} \dot{z}(t) + \{X_1 - X_{cg}, \dots, X_N - X_{cg}\} \dot{\epsilon}(t) \\ + \{\dot{q}_1(t), \dots, \dot{q}_k(t)\} \end{bmatrix} \begin{bmatrix} m_{11} & & \\ & m_{22} & \\ & & m_{NN} \end{bmatrix} \right\} \quad *$$

$$\begin{bmatrix} 1.0 \\ X_1 - X_{cg} \\ 1.0 \\ X_N - X_{cg} \end{bmatrix} \dot{z}(t) + \begin{bmatrix} X_1 - X_{cg} \\ X_N - X_{cg} \end{bmatrix} \dot{\epsilon}(t) + \begin{bmatrix} \phi_{11} & \phi_{12} & \dots & \phi_{1k} \\ \phi_{21} & \phi_{22} & \dots & \phi_{2k} \\ \vdots & \vdots & \ddots & \vdots \\ \phi_{N1} & \phi_{N2} & \dots & \phi_{Nk} \end{bmatrix} \begin{bmatrix} \dot{q}_1(t) \\ \dot{q}_2(t) \\ \vdots \\ \dot{q}_k(t) \end{bmatrix}$$

After simplification

$$T = \frac{1}{2} \left\{ \dot{z}, \dot{\epsilon}, \dot{q}_1, \dots, \dot{q}_k \right\} \begin{bmatrix} 1.0 & 1.0 & \dots & 1.0 \\ X_1 - X_{cg} & X_2 - X_{cg} & \dots & X_N - X_{cg} \\ \phi_{11} & \phi_{21} & \dots & \phi_{N1} \\ \vdots & \vdots & \ddots & \vdots \\ \phi_{1k} & \phi_{2k} & \dots & \phi_{Nk} \end{bmatrix} \begin{bmatrix} m_{11} & m_{11}(X_1 - X_{cg}) & m_{11}\phi_{11} & \dots & m_{11}\phi_{1k} \\ m_{22} & m_{22}(X_2 - X_{cg}) & m_{22}\phi_{21} & \dots & m_{22}\phi_{2k} \\ \vdots & \vdots & \vdots & \ddots & \vdots \\ m_{NN} & m_{NN}(X_N - X_{cg}) & m_{NN}\phi_{N1} & \dots & m_{NN}\phi_{Nk} \end{bmatrix} \begin{bmatrix} \dot{z} \\ \dot{\epsilon} \\ \dot{q}_1 \\ \vdots \\ \dot{q}_k \end{bmatrix} \quad (8)$$

Therefore

$$T = \frac{1}{2} \{\dot{n}\}^T [M] \{\dot{n}\} \quad (9)$$

where [M] is a (k+2) x (k+2) symmetric matrix whose elements are given by

$$M_{11} = \sum_{i=1}^N m_{1i} = m$$

where m is the total mass of the sled.

$$M_{22} = \sum_{i=1}^N m_{ii} (x_i - x_{cg})^2 = I$$

where I is the pitch inertia of the sled.

$$M_{jj} = \sum_{i=1}^N m_{ii} \phi_{i(j-2)}^2 \text{ for } j > 2$$

or

$$M_{jj} = \{\phi\}_{j-2}^T [m] \{\phi\}_{j-2}$$

Therefore M_{jj} is the generalized mass of the $(j-2)$ th mode for $j > 2$.

For $p > 2$, $l > 2$ and $p \neq l$,

$$M_{pl} = \sum_{i=1}^N \phi_{i(p-2)} m_{ii} \phi_{i(l-2)} = M_{lp} = 0$$

since the modes are orthogonal.

$$M_{12} = M_{21} = \sum_{i=1}^N m_{ii} (x_i - x_{cg}) = 0$$

because by definition the first moment of the masses about the cg of the body is zero.

$$M_{1j} = M_{j1} = \sum_{i=1}^N m_{ii} \phi_{i(j-2)} \text{ for } j > 2$$

$$M_{2j} = \sum_{i=1}^N (x_i - x_{cg}) m_{ii} \phi_{i(j-2)} = M_{j2} \text{ for } j > 2$$

Thus $[M]$ can be written as

$$[M] = \begin{bmatrix} m & 0 & M_{13} & \cdots & M_{1(k+2)} \\ & I & M_{23} & \cdots & M_{2(k+2)} \\ M_{13} & M_{23} & M_{33} & \cdots & 0 \\ \vdots & \vdots & \vdots & \ddots & \vdots \\ M_{1(k+2)} & M_{2(k+2)} & 0 & \cdots & M_{(k+2)(k+2)} \end{bmatrix} \quad (10)$$

The strain energy U is given by

$$U = \frac{1}{2} \{u\}^T [k] \{u\} \quad (11)$$

where $[k]$ is the stiffness matrix of the sled with respect to the degrees of freedom of the original finite element model. The strain energy with respect to the generalized coordinates $\{\eta\}$ can be written as

$$U = \frac{1}{2} \{\eta\}^T [K] \{\eta\} \quad (12)$$

where $[K]$ is a $(k+2) \times (k+2)$ matrix whose elements are given by

$$K_{11} = K_{22} = 0$$

since there is no strain energy in the rigid body motion.

$$K_{ij} = K_{ji} = 0 \quad i > 2, j > 2 \quad i \neq j$$

since $\{\phi\}_i$ and $\{\phi\}_j$ are orthogonal for $i \neq j$.

$$K_{ii} = \{\phi\}_i^T [k] \{\phi\}_i \quad i > 2 \quad j = i - 2$$

or

$$K_{ii} = M_{ii} \omega_j^2$$

where ω_j is the natural frequency of the j th mode, and M_{ii} is the generalized mass of the j th mode where i is $j+2$. Thus $[K]$ can be written as

$$[K] = \begin{bmatrix} 0 & & & 0 \\ & 0 & & \\ & & M_{33} \omega_1^2 & \\ 0 & & & M_{(k+2)(k+2)} \omega_N^2 \end{bmatrix} \quad (13)$$

Assuming that the damping forces are proportional to the generalized velocities, the Rayleigh Dissipation function is given in the form

$$F = \frac{1}{2} \{\dot{\eta}\}^T [C] \{\dot{\eta}\} \quad (14)$$

where $[C]$, the damping matrix, is assumed to be a $(k+2) \times (k+2)$ diagonal matrix of the form

$$[C] = \begin{bmatrix} 0 & & & & 0 \\ & 0 & & & \\ & & c_{33} & & 0 \\ & 0 & & 0 & \\ & & & & c_{(k+2)(k+2)} \end{bmatrix} \quad (15)$$

The work, W , is a product of the force in the slipper springs and the displacement of the attached structure. Since the attached structure was pinned in all the modes the springs do work only on the rigid displacements, z and θ . The forward and aft slipper forces are given by

$$F_F = -k_F \bar{\delta}_F(z + \ell_F \theta, \frac{\epsilon}{2} + Y(\bar{X} + \ell)) - D_F \quad (16)$$

$$F_A = -k_A \bar{\delta}_A(z - \ell_A \theta, \frac{\epsilon}{2} + Y(\bar{X})) - D_A \quad (17)$$

with the forward and aft spring forces given by

$$F_{F_S} = -k_F \bar{\delta}_F(z + \ell_F \theta, \frac{\epsilon}{2} + Y(\bar{X} + \ell))$$

and

$$F_{A_S} = -k_A \bar{\delta}_A(z - \ell_A \theta, \frac{\epsilon}{2} + Y(\bar{X}))$$

The definition of the $\bar{\delta}$ function is as follows:

$$\begin{aligned} \bar{\delta}(u, v) &= u - v, \quad u > v \\ &= 0, \quad |u| < v \\ &= u + v, \quad u < -v \end{aligned}$$

k_F and k_A are the forward and aft slipper support stiffnesses, respectively, ϵ is the slipper gap, ℓ_F and ℓ_A are distances from the sled cg to the slipper supports, Y is the rail height when the aft slippers are at down-track position \bar{X} , and ℓ is the distance between the forward and aft slippers. D_F and D_A , the damping forces, which act only when the slippers are in contact are given by

$$D_F = C_F(\dot{z} + \ell_F \dot{\theta} - vY'(\bar{X} + \ell)) \quad (18)$$

$$D_A = C_A(\dot{z} - \ell_A \dot{\theta} - vY'(\bar{X})) \quad (19)$$

where v is the sled downtrack velocity and Y' is the local slope of the railhead. The damping coefficients C_F and C_A are given by

$$C_F = (C_p + C_b) \frac{2k_F}{k_A + k_F} \quad (20)$$

$$C_A = (C_p + C_b) \frac{2k_A}{k_A + k_F} \quad (21)$$

where C_b , the damping coefficient at each slipper for bounce, is given by

$$C_b = \frac{1}{4} \left(2\xi_z \sqrt{(k_A + k_F)m} \right) \quad (22)$$

where m is the total mass of the sled and C_p , the damping coefficient at each slipper for pitch, is given by

$$C_p = \frac{1}{2(\ell_F^2 + \ell_A^2)} \left(2\xi_\theta \sqrt{I(k_A \ell_A^2 + k_F \ell_F^2)} \right) \quad (23)$$

where I is the pitch inertia of the sled. ξ_z and ξ_θ are the proportion of critical damping of bounce and pitch, respectively. The derivation of Eqs. (20) - (23) is given in Appendix A.

Thus the work, W , can be written as

$$W = \frac{F_F}{2} \bar{\delta}_F(u, v) + \frac{F_A}{2} \bar{\delta}_A(u, v) \quad (24)$$

Now that the terms associated with Eq. (6) have been found, it is possible to substitute Eq. (9) into Eq. (6) giving

$$\frac{\partial T}{\partial \dot{\eta}_i} = \sum_{j=1}^{k+2} M_{ij} \dot{\eta}_j \quad i = 1, 2$$

and

$$\frac{\partial T}{\partial \dot{\eta}_1} = \sum_{j=1}^2 M_{1j} \dot{\eta}_j + M_{11} \dot{\eta}_1 \quad i=3, \dots k+2$$

Therefore

$$\frac{d}{dt} \left(\frac{\partial T}{\partial \dot{\eta}_i} \right) = \sum_{j=1}^{k+2} M_{ij} \ddot{\eta}_j \quad i = 1, 2$$

and

$$\frac{d}{dt} \left(\frac{\partial T}{\partial \dot{\eta}_1} \right) = \sum_{j=1}^2 M_{1j} \ddot{\eta}_j + M_{11} \ddot{\eta}_1 \quad i=3, \dots k+2$$

Thus

$$\frac{d}{dt} \left(\frac{\partial T}{\partial \dot{\eta}} \right) = [M] \{\ddot{\eta}\} \quad (25)$$

Furthermore by substituting Eq. (12) into Eq. (6) for an arbitrary i , the expression for $\frac{\partial U}{\partial \eta_1}$ can be formulated as

$$\frac{\partial U}{\partial \eta_1} = K_{11} \eta_1$$

Again since i was arbitrary,

$$\frac{\partial U}{\partial \eta} = [K] \{\eta\} \quad (26)$$

If one substitutes Eq. (14) into Eq. (6) and observes that $[C]$ was assumed diagonal, then the calculation of $\frac{\partial F}{\partial \dot{\eta}_1}$ is the same as the calculation of $\frac{\partial U}{\partial \eta_1}$.

Therefore,

$$\frac{\partial F}{\partial \bar{n}} = [C]\{\dot{\bar{n}}\} \quad (27)$$

From Eq. (24), $W = W(z, \theta)$, therefore in Eq. (6)

$$\frac{\partial W}{\partial \eta} = \left\{ \frac{\partial W}{\partial z}, \frac{\partial W}{\partial \theta}, 0, \dots, 0 \right\}$$

From Eq. (24)

$$\begin{aligned} \frac{\partial W}{\partial z} &= \frac{1}{2} \frac{\partial F_F}{\partial z} \bar{\delta}_F(u, v) + \frac{1}{2} F_{F_S} \frac{\partial \bar{\delta}_F(u, v)}{\partial z} + \frac{1}{2} \frac{\partial F_{A_S}}{\partial z} \bar{\delta}_A(u, v) + \frac{1}{2} F_{A_S} \frac{\partial \bar{\delta}_A(u, v)}{\partial z} \\ &= \frac{1}{2} (-\bar{k}_F) \bar{\delta}_F(u, v) + \frac{1}{2} F_{F_S} + \frac{1}{2} (-k_A) \bar{\delta}_A(u, v) + \frac{1}{2} F_{A_S} \\ &= \frac{F_{F_S}}{2} + \frac{F_{F_S}}{2} + \frac{F_{A_S}}{2} + \frac{F_{A_S}}{2} \end{aligned}$$

Thus

$$\frac{\partial W}{\partial z} = F_{F_S} + F_{A_S} \quad (28)$$

Also from Eq. (24)

$$\begin{aligned} \frac{\partial W}{\partial \theta} &= \frac{1}{2} \frac{\partial F_F}{\partial \theta} \bar{\delta}_F(u, v) + \frac{1}{2} F_{F_S} \frac{\partial \bar{\delta}_F(u, v)}{\partial \theta} + \frac{1}{2} \frac{\partial F_{A_S}}{\partial \theta} \bar{\delta}_A(u, v) + \frac{1}{2} F_{A_S} \frac{\partial \bar{\delta}_A(u, v)}{\partial \theta} \\ &= \frac{1}{2} (-k_F l_F) \bar{\delta}_F(u, v) + \frac{1}{2} F_{F_S} l_F + \frac{1}{2} (-k_A) (-l_A) \bar{\delta}_A(u, v) + \frac{1}{2} F_{A_S} (-l_A) \\ &= \frac{F_{F_S} l_F}{2} + \frac{F_{F_S} l_F}{2} - \frac{F_{A_S} l_A}{2} - \frac{F_{A_S} l_A}{2} \end{aligned}$$

Thus

$$\frac{\partial W}{\partial \theta} = F_{F_S} l_F - F_{A_S} l_A \quad (29)$$

Then in matrix notation

$$\frac{\partial W}{\partial \eta} = \begin{Bmatrix} F_{F_S} + F_{A_S} \\ F_{F_S} \ell_F - F_{A_S} \ell_A \\ 0 \\ \vdots \\ 0 \end{Bmatrix} \quad (30)$$

The virtual work done by the damping forces D_F and D_A is given by

$$\delta W = D_F \vec{j} \cdot \delta(z + \ell_F \theta) \vec{j} + D_A \vec{j} \cdot \delta(z - \ell_A \theta) \vec{j}$$

Therefore

$$\delta W = (D_F + D_A) \delta z + (D_F \ell_F - D_A \ell_A) \delta \theta$$

Now $\delta z = \delta \eta_1$ and $\delta \theta = \delta \eta_2$, thus $Q_1 = D_F + D_A$ and $Q_2 = D_F \ell_F - D_A \ell_A$

Then in matrix notation the nonconservative forces are given by

$$Q = \begin{Bmatrix} D_F + D_A \\ D_F \ell_F - D_A \ell_A \\ 0 \\ \vdots \\ 0 \end{Bmatrix} \quad (31)$$

From Eqs. (30) and (31) the forcing function $\{F\}$ is given by

$$\{F\} = \frac{\partial W}{\partial \eta} + Q = \begin{Bmatrix} (F_{F_S} - D_F) + (F_{A_S} - D_A) \\ (F_{F_S} \ell_F - D_F \ell_F) - (F_{A_S} \ell_A - D_A \ell_A) \\ 0 \\ \vdots \\ 0 \end{Bmatrix} = \begin{Bmatrix} F_F + F_A \\ F_F \ell_F - F_A \ell_A \\ 0 \\ \vdots \\ 0 \end{Bmatrix} \quad (32)$$

by Eqs. (16) and (17).

Combining Eqs. (25), (26), (27), and (32) the equations of motion can now be written as

$$[M]\{\ddot{\eta}\} + [C]\{\dot{\eta}\} + [K]\{\eta\} = \{F\} \quad (33)$$

where matrices $[M]$, $[C]$ and $[K]$ and vector $\{F\}$ are defined by Eqs. (10), (15), (13) and (32) respectively and $\{\eta\} = \{z, \theta, q_1, q_2, \dots, q_k\}$

As a final step in determining the coefficient matrices in Eq. (33), it becomes necessary to formulate the $[C]$ matrix corresponding to the elastic modes. Since the rigid body vertical translation, z , and rotation, θ , are uncoupled from the normal coordinates, q_i , $i=1, \dots, k$, Eq. (33) can be rewritten as

$$\begin{bmatrix} M_{33} & 0 & 0 \\ 0 & M_{44} & 0 \\ 0 & 0 & M_{(k+2)(k+2)} \end{bmatrix} \begin{Bmatrix} \ddot{q}_1 \\ \ddot{q}_2 \\ \ddot{q}_k \end{Bmatrix} + \begin{bmatrix} C_{33} & 0 & 0 \\ 0 & C_{44} & 0 \\ 0 & 0 & C_{(k+2)(k+2)} \end{bmatrix} \begin{Bmatrix} \dot{q}_1 \\ \dot{q}_2 \\ \dot{q}_k \end{Bmatrix} + \begin{bmatrix} M_{33}\omega_1^2 & 0 & 0 \\ 0 & M_{44}\omega_2^2 & 0 \\ 0 & 0 & M_{(k+2)(k+2)}\omega_k^2 \end{bmatrix} \begin{Bmatrix} q_1 \\ q_2 \\ q_k \end{Bmatrix} = 0 \quad (34)$$

Eqs. (34) represents k uncoupled differential equations. For any i Eqs. (34) can be written

$$M_{ii}\ddot{q}_{i-2} + C_{ii}\dot{q}_{i-2} + M_{ii}\omega_{i-2}^2 q_{i-2} = 0 \quad i = 3, \dots, k+2 \quad (35)$$

Assume $[C] = 2\gamma[M]$ where γ is a proportionality constant.⁽⁷⁾ Then Eq. (35) becomes

$$M_{ii}\ddot{q}_{i-2} + 2\gamma M_{ii}\dot{q}_{i-2} + M_{ii}\omega_{i-2}^2 q_{i-2} = 0 \quad (36)$$

Thus if $q_{i-2} = Ae^{st}$, the characteristic equation becomes

$$M_{ii}As^2e^{st} + 2\gamma M_{ii}Ase^{st} + M_{ii}\omega_{(i-2)}^2Ae^{st} = 0$$

or

$$(s^2 + 2\gamma s + \omega_{(i-2)}^2)Ae^{st} = 0 \quad (37)$$

The roots of Eq. (37) are given by

$$s = -\gamma \pm \sqrt{\gamma^2 - \omega_{i-2}^2} \quad (38)$$

For the critically damped case, $\gamma^2 - \omega_{i-2}^2 = 0$, i.e. $\gamma_0 = \omega_{i-2}$ where γ_0 is the value of γ corresponding to the critically damped system. Then $\frac{\gamma}{\gamma_0} \geq 1$ represents the overdamped, critically damped and underdamped systems respectively. If ξ_{i-2} is assumed to be $\frac{\gamma}{\gamma_0}$, then the damping coefficients can be written as

$$C_{ii} = 2\gamma M_{ii} = 2 \frac{\gamma}{\gamma_0} \omega_{(i-2)} M_{ii}$$

or

$$C_{ii} = 2\xi_{(i-2)}\omega_{(i-2)}M_{ii} \quad (39)$$

Thus the elements of Eqs. (33) are completely defined. Additional quasi-steady forces and moments, F_s and M_s , are included in the definition of $\{F\}$, Eq. (32), such that

$$\{F\} = \begin{Bmatrix} F_F + F_A + F_S \\ F_F l_F - F_A l_A + M_S \\ 0 \\ \vdots \\ 0 \end{Bmatrix} \quad (40)$$

A discussion of these forces is given in Ref. 5. Eqs. (33) represents a system of $(k+2)$ second order differential equations, the solution of which will be discussed in the next section.

III. DESCRIPTION OF AN INTEGRATED DESIGN TOOL

A schematic of the design process is given in Fig. 4. The purpose of the scheme is to establish communication between two main programs. The first program, "NASTRAN" is a finite element program which can solve static and dynamic structural analysis problems.^{(8),(9)} The second program, "SLEDYNE" numerically integrates the reduced system of equations (Eqs. 33) by a predictor corrector method. The program SGAMT provides communication between NASTRAN and SLEDYNE. Similarly the program SLEDNAS transmits data from SLEDYNE to NASTRAN for a static analysis.

In the derivation of the equations of motion, Eqs. (33) the normal modes of vibration $\{\phi\}_i, i=1, \dots, k$, the natural frequencies ω_i , the generalized masses and the diagonal matrix of the lumped masses $[m]$ were assumed to be known. This information was obtained by conducting a free vibration analysis of the sled restrained against translation at the slipper support points. The sled was modeled using finite elements, and a normal mode analysis was made with the NASTRAN program, rigid format #3, using the inverse power method. The Nastran finite element model definition, natural frequencies ω_i and normal mode shapes $\{\phi\}_i$, lumped mass matrix $[m]$ and the generalized masses are reformatted via the translator program SGAMT to SLEDYNE requirements.

Eqs. (33) are solved by the "SLEDYNE" program. The program computes the time history dynamic response of a sled traversing on a track which has roughness characteristics derived from sample track measurements. In addition to mass, frequency and mode shape data SLEDYNE requires aerodynamic data in the form of time histories of thrust, lift, drag and center of lift. Additional data required for definition of the sled geometry is given in Fig. 5. The system of $(k+2)$ second order differential

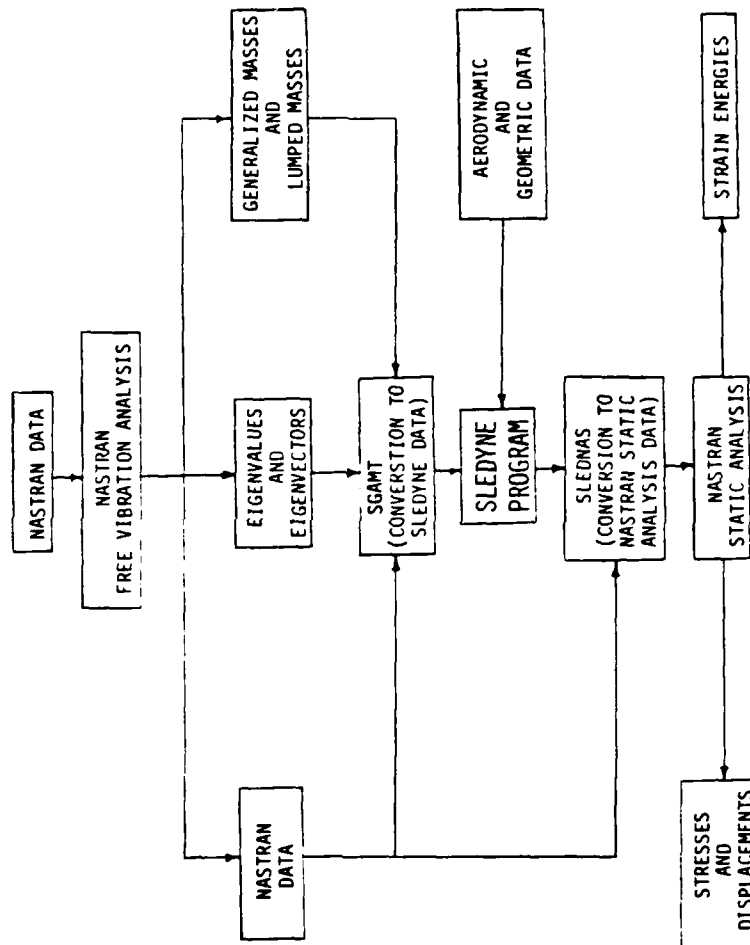
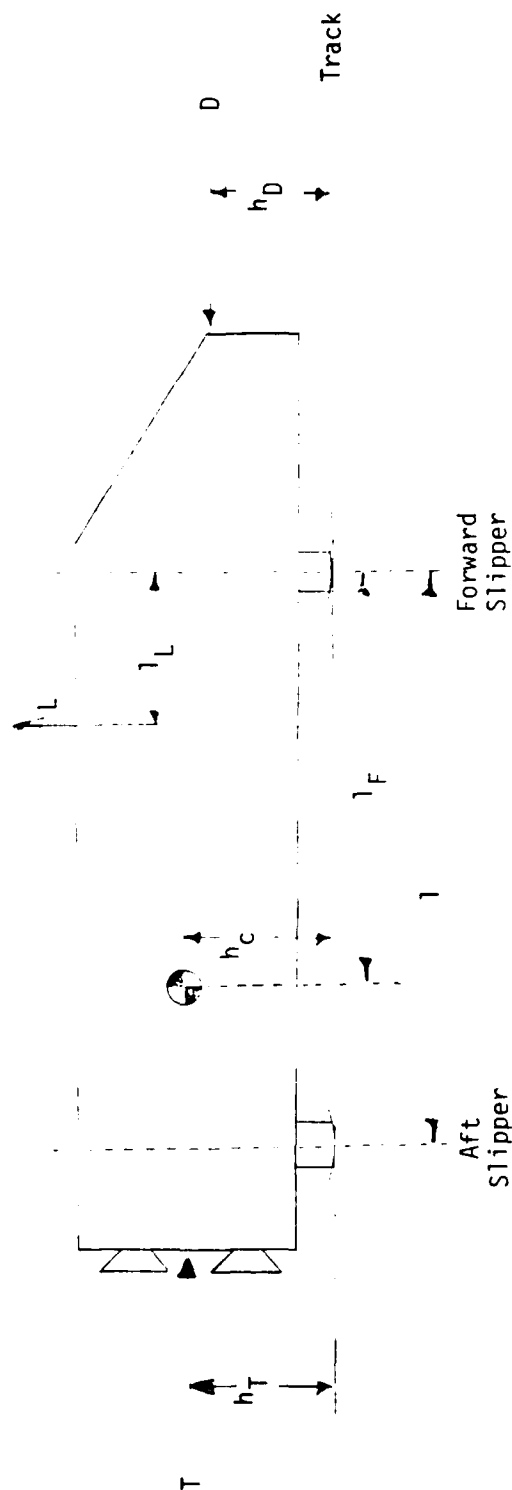


Figure 4. Integrated Design Tool

Figure 5. Sled Geometry



Symbol	Description*
L	Lift on the Sled
T	Thrust
D	Drag
l	Distance Between the Forward and Aft Slippers
l_L	Distance From the Forward Slipper to the Center of Lift
l_F	Distance From the Forward Slipper to cg
h_T	Height of Center of Thrust Above the Rail Head
h_D	Height of the Center of Drag
h_C	Height of the cg Above Rail Head

* UNITS ARE IN INCHES OR POUNDS

equations is reduced to a set of $2(k+2)$ first order differential equations. The fourth order Adams-Moulton predictor corrector method based on the classical fourth order Runge-Kutta method was used for the time integration. (10), (11)

The most important SLEDYNE results are a set of force vectors. These are the inertial forces acting on all the mass points of the sled. For each slipper at the peak time, the vector of accelerations of the independent variables, $(\ddot{z}, \ddot{\theta}, \ddot{q}_1, \dots, \ddot{q}_k)$ is used to calculate the inertial loads by the following equation

$$\{F_I\} = - [m] \begin{Bmatrix} 1.0 \\ \vdots \\ 1.0 \end{Bmatrix} \ddot{z}(t) + \begin{Bmatrix} X_1 - X_{cg} \\ \vdots \\ X_N - X_{cg} \end{Bmatrix} \ddot{\theta}(t) + \begin{bmatrix} \phi_{11} & \phi_{12} & \dots & -\phi_{1k} \\ \phi_{21} & \phi_{22} & \dots & -\phi_{2k} \\ \vdots & \vdots & & \vdots \\ \phi_{N1} & \phi_{N2} & \dots & -\phi_{Nk} \end{bmatrix} \begin{Bmatrix} \ddot{q}_1 \\ \ddot{q}_2 \\ \vdots \\ \ddot{q}_k \end{Bmatrix} \quad (41)$$

The inertial forces obtained from the SLEDYNE program and the original finite element model are integrated by the SLEDNAS Program to generate data for a NASTRAN static analysis. A NASTRAN static strength analysis is performed, and the response of the sled to the inertial loads is measured via the total strain energy of the sled, the stresses in the elements and the displacements at the nodes. It is possible that with the obtained data the adequacy of the sled, with respect to strength, could be evaluated.

IV. SIMULATION OF RAIL ROUGHNESS PROFILES

The values of rail roughness $Y(\bar{X})$ and $Y(\bar{X}+l)$ were required when evaluating the forward slipper force F_F and the aft slipper force F_A defined in Eqs. (16) and (17), respectively. The rail roughness model used in SLEDYNE is based on a set of 430 measurements made of rail height on a 400 ft section of the Holloman track. The data from this 400 ft track is used as a sample to generate a rail roughness profile for the entire track. The description of how this data is generated is not clear in Ref. 5. The following discussion is based on a direct reading and interpretation of the SLEDYNE program.

The measurements were divided into ten unequal segments such that the first value of each segment is zero. The ten segments were arbitrarily assigned the following number of measurements, respectively: 41, 61, 48, 40, 44, 36, 31, 21, 63, and 45. The rail roughness profile for the length of track needed for each SLEDYNE run is constructed randomly from these ten segments. The sled downtrack velocity, v , and the total time of the run, t_f , are required SLEDYNE data. Since the total distance, \bar{X}_T , that the sled will travel is

$$\bar{X}_T = vt_f + 100 \quad (42)$$

a rail roughness profile will have to be defined to cover that length of track. The factor 100 is simply to assure an adequate length of track. SLEDYNE internally generates this profile (which will be referred to as the original SLEDYNE profile) as follows.

To define the segments in the profile, the program uses a random number generator function $y=\text{RANF}(A)$, which gives a random value of y such that $0 < y < 1$ for every function call. Thus,

$$J = [10y + 1] \quad (43)$$

is an integer such that $1 \leq J \leq 10$, where $[]$ is the greatest integer function. So for every value of y the corresponding J th segment is included in the profile. The order of the segments as well as a count, NC , of the total number of measurements defining the profile is maintained internally. The profile is completely generated when $NC = [(vt_f + 100)(1.2) + 1]$. The factor 1.2 simply refers to a 20% increase in the length of the track to be covered. Now the total travel distance is divided into NC divisions, and the rail height is available at each of these divisions. For the integration of Eqs. (33) each of these NC divisions is further divided into ten parts, and the response of the sled is computed at 10 NC points.

For a dual rail sled two profiles are generated, one for each rail. Profile generation is completed before the solution of Eqs. (33) begins. On CDC computers RANF(A) generates the same sequence of random numbers every time. Thus for every SLEDYNE run the same profiles will be generated, they only vary as to their length. The SLEDYNE rail roughness profile for the right rail for the first 3 selected segments is given in Fig. 6.

The values of $Y(\bar{X})$ and $Y(\bar{X}+1)$ for a given value of \bar{X} is obtained from the rail roughness profile generated earlier. For example, the rail height $Y(\bar{X})$ at a distance \bar{X} is computed by the straight line interpolation

$$Y(\bar{X}) = y_0 + \frac{y_1 - y_0}{x_1 - x_0} (\bar{X} - x_0) \quad (44)$$

The quantities y_0 and y_1 are the rail heights at distances x_0 and x_1 , which are defined as

$$x_0 \leq \bar{X} < x_1$$

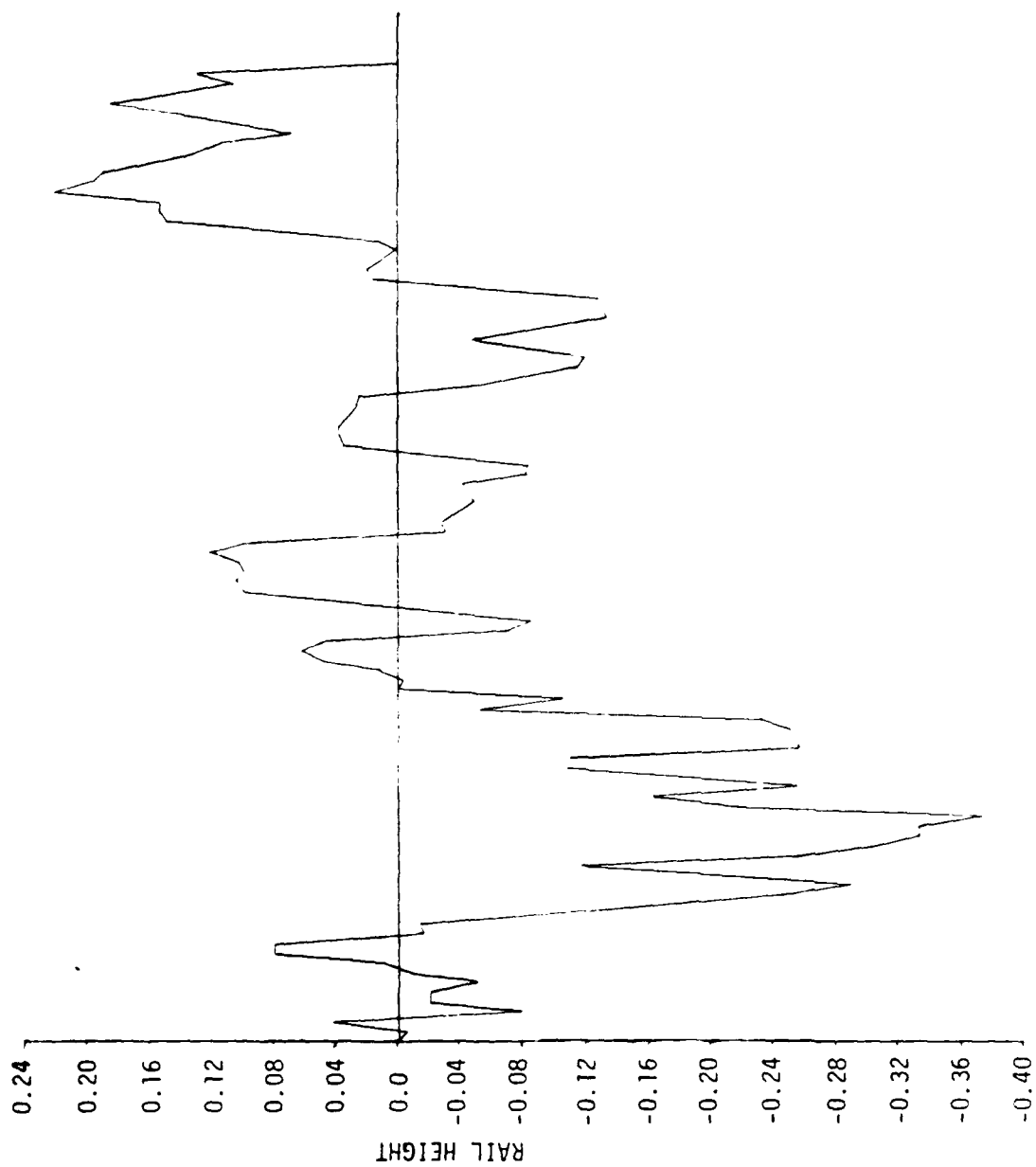


FIGURE 6. SLEDYNE RAIL ROUGHNESS PROFILE FOR THE RIGHT RAIL

The actual locations of x_1 and x_0 are determined as follows:

A parameter N^* is defined as

$$N^* = \left[\frac{\bar{X}}{10} + 1 \right] \quad (45)$$

where $[]$ is the greatest integer function.

Then

$$x_1 = 10N^* \quad \text{and} \quad x_0 = 10(N^* - 1)$$

This interpolation is necessary because the rail heights are available only at every 10th integration point. The rail height for the forward slipper $Y(\bar{X}+1)$ is computed in a similar manner.

Initially, of course, at $t=0$, $y_0=0$ and y_1 = the second entry of the first segment of the profile. At time $t=t_1$, $y_0=y_1$ and y_1 = the third entry of the first segment of the profile.

The author recognizes that SLEDYNE'S random approach toward rail roughness is really not random enough. It is felt that a profile function should be associated with each individual slipper. Thus, the Monte Carlo approach was chosen as an alternate procedure for generating a rail roughness profile. (12, (13), (14)) By definition "Monte Carlo" refers to an approach for reconstructing probability distributions based on the selection or generation of random numbers. The original SLEDYNE profile was generated based on a set of 430 rail measurements. This set of measurements was designated by $\{V_i\}$, $i=1, \dots, 430$. For the Monte Carlo approach the $\{V_i\}$ was normalized by V_{\max} where $|V_i| \leq |V_{\max}|$ for all i . Thus $-1 \leq V_i \leq 1$. A sequence of j intervals were arbitrarily defined between $[-1, 1]$, and the mean value, VAL_j , was assigned to each interval (See Columns 1 and 2 of Table 1). The probability distribution of rail measurements given in Column 4 was generated in the following manner: The number of elements

INTERVAL x (1)	VALUE (2)	FREQUENCY OF OCCURRENCE (3)	PMF f(x) (4)	CDF F(x) (5)	RANGE ALONG 0-1 SCALE (6)
[-1.00, -.95)	-1.0	3	.01	.01	0.00- .01
[-.95, -.85)	-.9	5	.01	.02	.01- .02
[-.85, -.75)	-.8	10	.02	.04	.02- .04
[-.75, -.65)	-.7	13	.03	.07	.04- .07
[-.65, -.55)	-.6	13	.03	.10	.07- .10
[-.55, -.45)	-.5	7	.02	.12	.10- .12
[-.45, -.35)	-.4	11	.03	.14	.12- .14
[-.35, -.25)	-.3	21	.05	.19	.14- .19
[-.25, -.15)	-.2	31	.07	.27	.19- .27
[-.15, -.05)	-.1	49	.11	.38	.27- .38
[-.05, .05)	.0	62	.14	.52	.38- .52
[.05, .15)	.1	59	.14	.66	.52- .66
[.15, .25)	.2	37	.09	.75	.66- .75
[.25, .35)	.3	38	.09	.83	.75- .83
[.35, .45)	.4	29	.07	.90	.83- .90
[.45, .55)	.5	24	.06	.96	.90- .96
[.55, .65)	.6	9	.02	.98	.96- .98
[.65, .75)	.7	9	.02	1.00	.98-1.00

Table 1. Probability Distribution of Rail Roughness

of $\{V_i\}$ which occurred in each interval was recorded under Frequency of Occurrence, $FREQ_j$ (Column 3), and the probabilities PMF_j calculated by

$$PMF_j = \frac{FREQ_j}{430}$$

The Cumulative Distribution Function, CDF_k (Column 5), was calculated by

$$CDF_k = \sum_{j=1}^k PMF_j, k=1, \dots, \text{No. of intervals. For every } k \text{ a range along the}$$

0-1 scale was defined (See Column 6 of Table 1). Table 1 is the basis for the Inverse Transformation Method for generating random variates.

The Inverse Transformation Method can be explained as follows: In statistical terminology, if \overline{XX} denotes a random variable and x_j is a specific value of the random variable, then the probability mass function (PMF_j) can be defined as

$$f(x_j) = P(\overline{XX} = x_j)$$

such that

$$0 \leq f(x_j) \leq 1$$

and

$$\begin{array}{l} \text{NO. OF INTERVALS} \\ \sum_{j=1} f(x_j) = 1 \end{array}$$

where $P(\overline{XX}=x_j)$ is the probability that the random variable \overline{XX} takes on a value of x_j . For example the probability that the rail height takes on a value 0.1 is 0.14 or $P(\overline{XX}=0.1)=0.14$, $P(\overline{XX}=0.2)=0.09$ and so on. The Inverse Transformation Method consists of generating another random variable U' which is uniformly distributed over the range $[0,1]$. Then by definition $P(0 \leq U' < 0.01)=0.01$, $P(0.01 \leq U' < 0.02)=0.01$, $P(0.02 \leq U' < 0.04)=0.02$ and so on (See Columns 6 and 4). Since the probabilities for the given ranges of

U' are respectively identical to the probabilities for the given values of \overline{XX} , it follows that U' can be used to simulate or "artificially reconstruct" occurrences of \overline{XX} from Table 1.

The random number generator function RANF(A) is used to generate a rail roughness profile (called the Monte Carlo profile) using the Monte Carlo technique. A Monte Carlo profile is generated independently for each slipper and in real time as the sled is moving down the track, i.e. at the same time that Eqs. (33) are being integrated.

Now the rail roughness profile by the Monte Carlo approach can be generated by using Table 1. At a time $t=t_s$ the sled has travelled \overline{X}_s feet along the rails where \overline{X}_s is the downtrack position of the aft slipper. Using the random number generator, the value of U' is determined by $U' = \text{RANF}(A)$. Now the value of U' is located in the interval R along the 0-1 scale (Column 6) of Table 1. The corresponding j interval and VAL_j are identified from Column 2. The values of N^* , x_0 , x_1 and $Y(\overline{X}_s)$ are calculated by Eqs. (44) and (45). Similarly the value of $Y(\overline{X}_s + \ell)$ is determined corresponding to the distance $\overline{X}_s + \ell$. As in the original SLEDYNE profile, the rail roughness value Y corresponding to the intermediate value of X is found by linear interpolation between two consecutive values of the profile. The Monte Carlo rail roughness profile for the right forward slipper for the first 100 points is given in Fig. 7. Another method of defining rail roughness is given in Ref. 15.

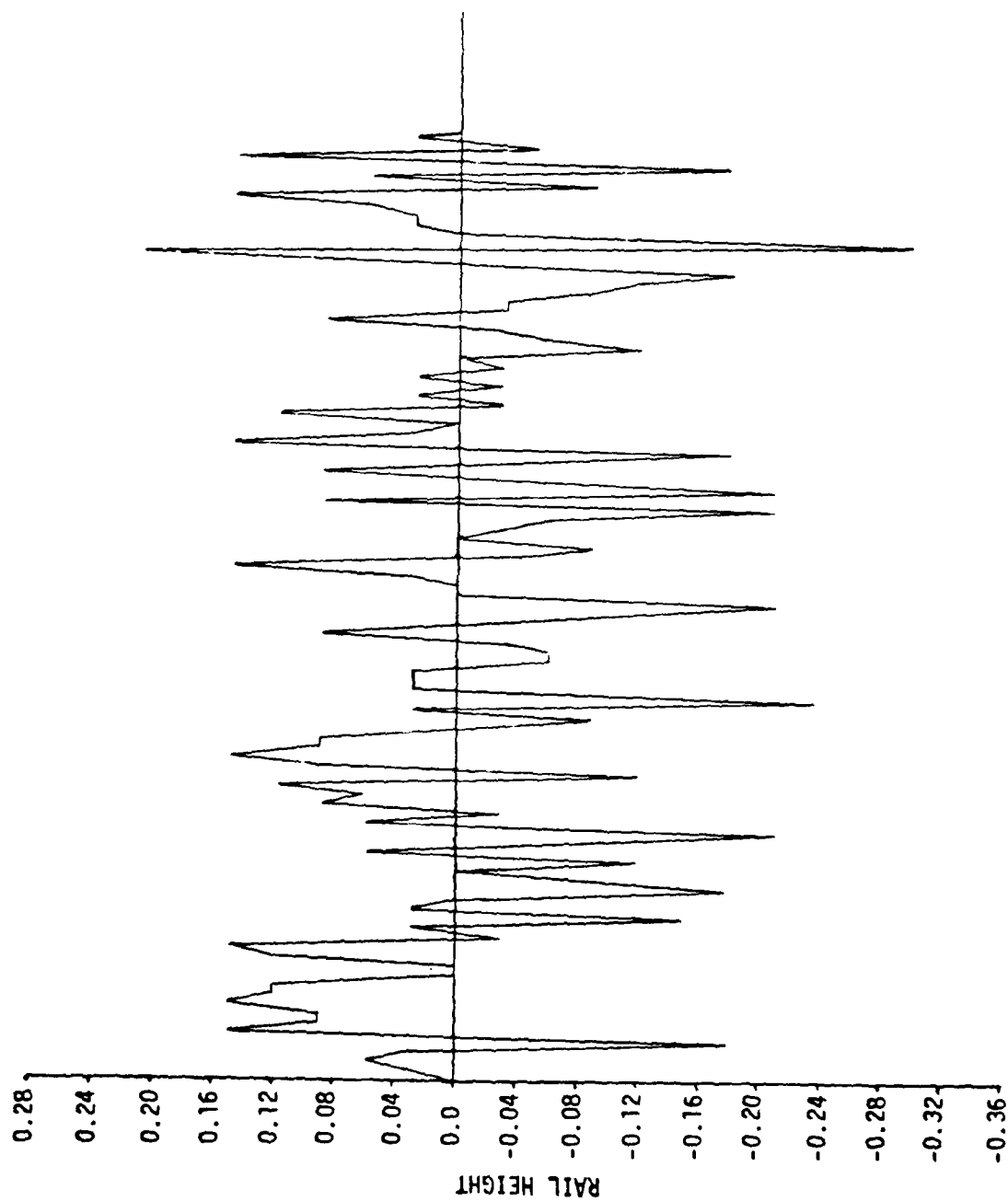


FIGURE 7. MONTE CARLO RAIL ROUGHNESS PROFILE FOR THE RIGHT FORWARD SLIPPER

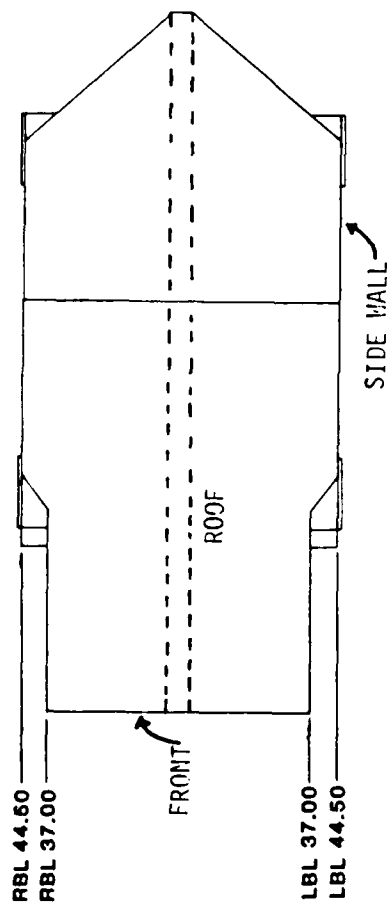
V. RESULTS

This section is divided into two parts. The first part describes the finite element model of a particular sled. In the second part a dynamic analysis of the sled is conducted and its response to a variation in both slipper stiffnesses k_A and k_F and rail roughness profile is examined.

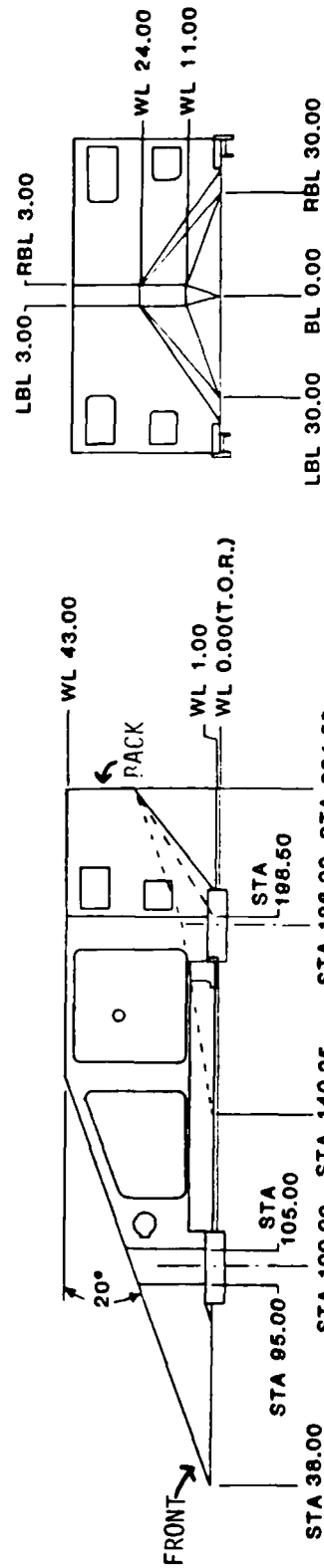
Model Description

The MX forebody configuration A rocket sled was chosen for this study. The general arrangement of this sled is given in Fig. 8. Configuration A was designed as a high frequency sled with a fundamental frequency of approximately 100HZ without payload masses. The sled forebody consists of a roof, a floor, two side walls and an intermediate wall at the center running longitudinally and three transverse bulkheads. All these components are constructed primarily of aluminum honeycomb panels with different face sheet thicknesses and core cell sizes. (16)(17)

Initially all the honeycomb panels were modeled with sandwich elements. In NASTRAN, QUAD1 and TRIA1, the quadrilateral and triangular elements respectively, were chosen to model the sandwich elements. The fin structure in the front (See Fig. 9) was modeled with homogeneous quadrilateral and triangular elements, QUAD2 and TRIA2. All of these elements have both inplane and bending stiffnesses. The finite element model with 53 nodes and 63 elements is shown in Fig. 9. The model has three longitudinal bulkheads and four transverse bulkheads. The sandwich elements modeling the floor had a face sheet thickness of .144" with a 1.856" core. The remaining sandwich elements in the bulkheads and on top of the sled had a face sheet thickness of .126" with a 1.874" core. The homogeneous elements modeling the front fin of the sled were .19" thick.



TOP VIEW



SIDE VIEW

BACK VIEW

Figure 8. GENERAL ARRANGEMENT - MX FOREBODY CONFIGURATION A

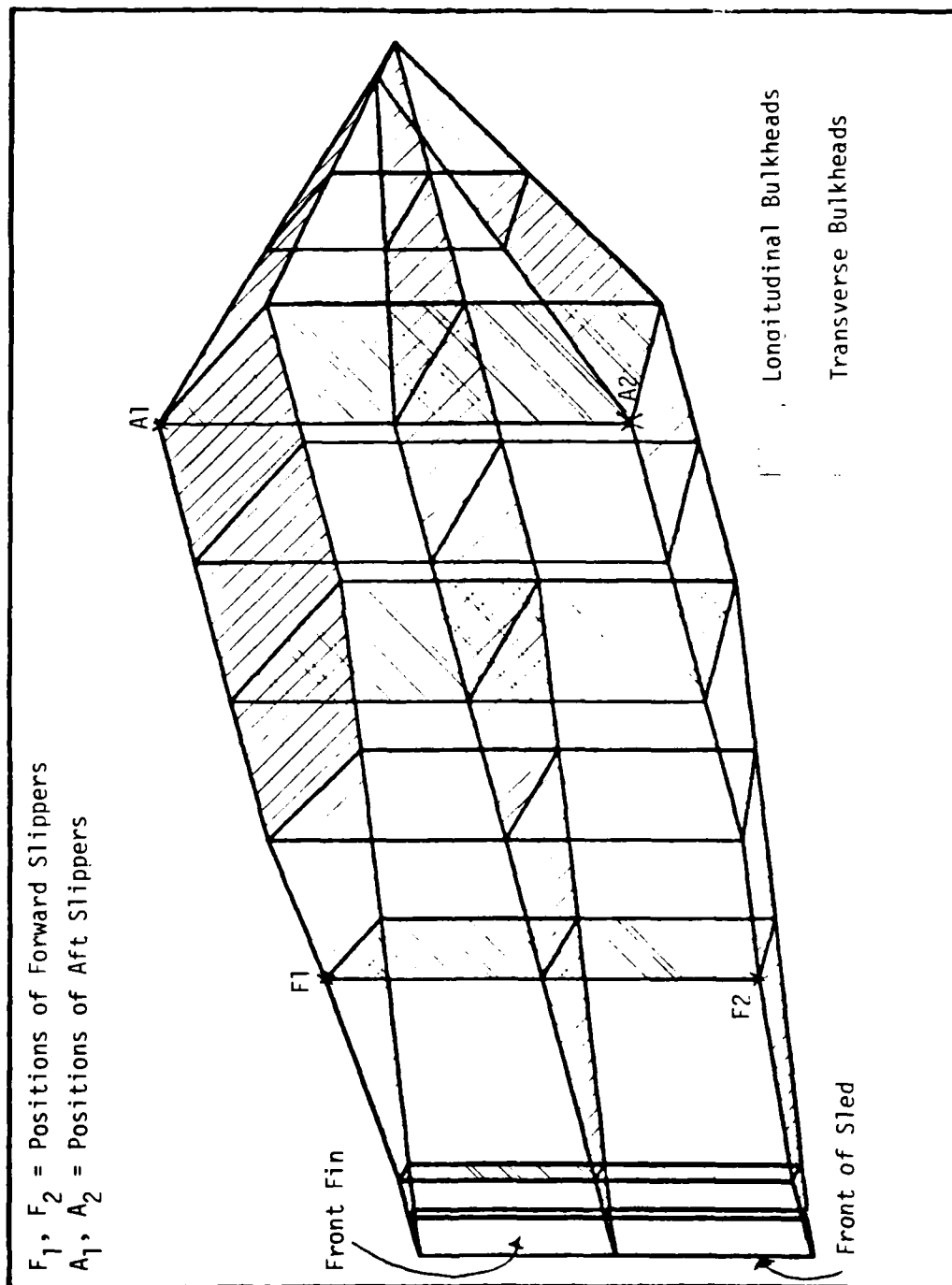


Figure 9. Finite Element Model of the MX Forebody Configuration A

The position of the four slippers on the sled is indicated by an * in Fig. 9. Each slipper is identified by a viewer positioned on top of the sled facing the front of the sled. F1 implies forward slipper 1, F2 implies forward slipper 2, A1 implies aft slipper 1 and A2 implies aft slipper 2. Note that the viewer position implies that F1 and A1 will ride the right rail.

Realistically this model overestimated the stiffness and indicated a fundamental frequency of approximately 150HZ. This overestimation of stiffness is a result of the constant strain triangles and quadrilaterals used to construct the sandwich elements in the bulkheads. Since the bulkheads have high stress gradients, these elements overestimate their stiffness.⁽¹⁸⁾ In order to obtain more realistic frequencies, the sandwich elements in the bulkheads in the revised model were replaced by aluminum SHEAR and ROD elements. The final model had 53 nodes and 98 elements and is also illustrated by Fig. 9. The fundamental frequency of this sled is approximately 103HZ.

Dynamic Analysis Results

The parametric study in this section involves variation of the rail roughness profile and the slipper stiffnesses. Both of these affect only the right hand side of Eqs. (33), which includes the forward and aft slipper forces (See Eqs. 16-23). In Section 4 two different rail roughness profiles were defined, the original SLEDYNE profile and the Monte Carlo profile. For each of these rail roughness profiles the slipper stiffnesses k_A and k_F will be varied in determining the response of the sled. The dynamic analysis of the sled was conducted in accordance with Fig. 4.

Initially a Nastran free vibration analysis was performed on the sled

model, and the first 6 frequencies and corresponding mode shapes are given in Fig. 10. The mode shapes and the undeformed sled are indicated by dashed and solid lines, respectively. It would appear that the mode shapes realistically depict the natural frequencies normally associated, through experience, with this type of vehicle. The frequencies λ_1 , λ_2 , λ_3 , and λ_6 clearly depict vertical bending modes while λ_4 and λ_5 pictorially represent in-plane bending modes. These mode shapes, their generalized masses, the matrix of lumped masses, and the Nastran data were integrated and reformed by the translator SGMAT for Program SLEDYNE as shown in Fig. 4.

The aerodynamic and geometric data required by SLEDYNE (See Fig. 5) were provided by Holloman Air Force Base. The velocity of the sled, v , was 2000 ft/sec and the total time of the run, t_f , was 2.001 seconds. The baseline values of slipper stiffnesses (supplied by Holloman) were $k_F = k_A = 96.0 \times 10^4$. Additional values of slipper stiffnesses for parametric study were chosen as $k_A = k_F = 48.0 \times 10^4$ and $k_A = k_F = 192.0 \times 10^4$. Thus, six SLEDYNE runs were made: The original SLEDYNE profile with three separate values of slipper stiffness and the Monte Carlo profile with three separate values of slipper stiffness.

For the original SLEDYNE profile for each value of slipper stiffness, the vector of accelerations of the independent variables, $(\ddot{z}, \ddot{\theta}, \ddot{q}_1, \dots, \ddot{q}_6)$ is given in Table 2a at that time when the dynamic force is a maximum for each slipper. Here slipper 1 implies forward slipper 1, slipper 2 implies forward slipper 2, slipper 3 implies aft slipper 1 and slipper 4 implies aft slipper 2. (See Fig. 9). Accelerations \ddot{q}_4 and \ddot{q}_5 are zero since modes 4 and 5 were in-plane bending modes which do not contribute to the vertical displacement $w(x,t)$ of the sled. These acceleration vectors are used to calculate the inertial loads by Eq. (41). Note that for a given value of

slipper stiffness $k_A = k_F$, the peak times vary for each slipper. Also as k_A and k_F increase, the peak time for the same slipper changes. For increasing values of stiffness, the vertical acceleration \ddot{z} increases in absolute value for the forward and aft slipper 2, while \ddot{z} assumes its maximum value at $k_F = k_A = 96 \times 10^4$ for the forward and aft slipper 1. The results imply that the slippers on each rail move in the same direction due basically to the similarities of the rail roughness profile on the same rail.

In considering the rail roughness profile contribution to the moving vehicle, it would appear that when one considers a set of slippers on a given side, one would see like movement. But to determine this, data for a constant value of slipper stiffness $k_A = k_F$ must appear with the peak time comparisons approximately equal. This does occur in Table 2a for $k_A = k_F = 48.0 \times 10^4$ at a peak time of ≈ 1.4 . Realistically speaking, one would assume that this type of phenomena would actually occur due to the stiffness of the vehicle. It is very strong in bending resistance as observed by the insignificant values of $\ddot{\theta}$.

Table 2b gives the vector of accelerations of the independent variables, $(\ddot{z}, \ddot{\theta}, \ddot{q}_1, \dots, \ddot{q}_6)$ for the Monte Carlo profile. As in Table 2a the absolute value of $\ddot{\theta}$ is small for all values of stiffness. In this table for increasing values of stiffness the vertical acceleration \ddot{z} increases in absolute value for the forward slippers 1 and 2 and the aft slipper 2, while \ddot{z} has its maximum value at $k_F = k_A = 96 \times 10^4$ for the aft slipper 1. A different rail roughness profile was generated for each slipper when using the Monte Carlo technique. Thus each slipper experiences a different profile.

From Tables 2a and 2b there will be a set of inertial loads for each value of slipper stiffness for each slipper, i.e. 24 sets. Each set of inertial loads was integrated separately with the NASTRAN data from the

free vibration analysis and reformatted by Program SLEDNAS for a NASTRAN static analysis as shown in Fig. 4.

A NASTRAN static analysis was performed for each set of inertial loads and the response measured in two ways: The total strain energy of the sled and plots of the deformed sled. For the original SLEDYNE profile Table 3a gives the total strain energy of the sled in in-lb for each value of slipper stiffness for each slipper. Table 3b gives the corresponding results for the Monte Carlo profile. In general for each profile the total strain energy increases with increasing values of slipper stiffness $k_A = k_F$. And this becomes more obvious when the peak times for the same slipper are approximately equal. An exception is noted for the original SLEDYNE profile for forward slipper 1 when $k_A = k_F = 96 \times 10^4$, and for the Monte Carlo profile for aft slipper 1 when $k_A = k_F = 192 \times 10^4$. In both cases the strain energy decreased as the stiffness increased. This phenomena implies that the total inertial load at the mass points of the sled decreased from that generated for the previous value of stiffness. It is possible that for any given value of stiffness, the contribution of the vertical acceleration \ddot{z} offsets the contribution of the elastic mode accelerations, thus resulting in lower inertial loads. The inertial loads calculated by Eq. (41) are a function of the maximum accelerations given in Tables 2a and 2b.

For the original SLEDYNE profile Figs. 11, 12, and 13 give the deformed shape of the sled superimposed on the undeformed shape for the indicated value of slipper stiffness. As before the deformed sled is drawn with dashed lines while the original sled is drawn with solid lines. Deformation plots A correspond to the inertial loads calculated for forward slipper 1; deformation plots B correspond to the inertial loads calculated for aft slipper 1; deformation plots C correspond to the inertial loads

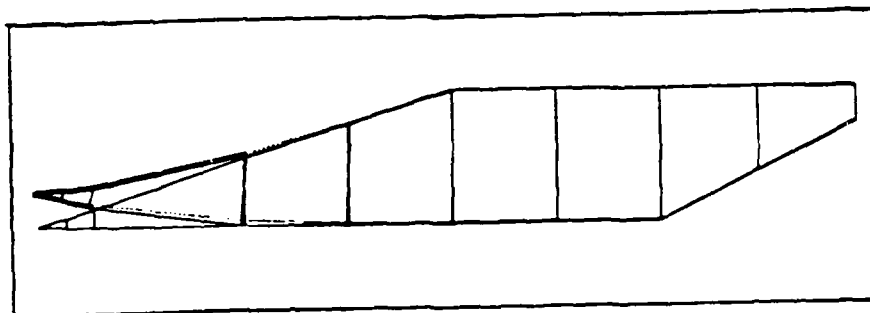
calculated for forward slipper 2, and deformation plots D correspond to the inertial loads calculated for aft slipper 2. Some observations can be made about the deformation plots by studying Fig. 11. Upon examining the accelerations in Table 2a for the forward slipper 1, one can observe that not only $\ddot{z}=.0933$ is small in absolute value compared to $\ddot{q}_1=-.4320$, but also \ddot{q}_1 exceeds by a minimum of 70% the magnitude of the remaining elastic mode accelerations. Thus from Eq. (41), the contribution of the first mode in calculating the inertial loads far exceeds that of the rigid body modes and the remaining elastic modes. This contribution is evident if Fig. 11A is compared with the first mode given in Fig. 10. Similarly, examining Table 2a for the aft slipper 1, the contribution of \ddot{z} , \ddot{q}_1 and \ddot{q}_3 is noted, and a comparison of Fig. 11B and Fig. 10 for modes 1 and 3 can be made. For the forward slipper 2, Table 2a gives the largest maximum accelerations as $\ddot{q}_1=-.3785$ and $\ddot{q}_6=.2214$. However, comparing Fig. 11C and Fig. 10, the contribution of the first mode appears to be predominant compared to the sixth mode. For aft slipper 2, Table 2a gives the largest maximum accelerations as $\ddot{q}_1=.5553$ and $\ddot{q}_6=-.3554$. In this case comparing Fig. 11D and Fig. 10, the influence of the sixth mode is comparable to the first mode. Similar observations could also be made for Figs. 12 and 13. Figs. 14, 15, and 16 give deformation plots for the Monte Carlo profile for the indicated value of stiffness. In general the deformation plots reflect the contribution of the mode shapes to the inertial loads, Eqs. (41).

In examining the results shown in Tables 2a, 2b, 3a and 3b two points should be considered.

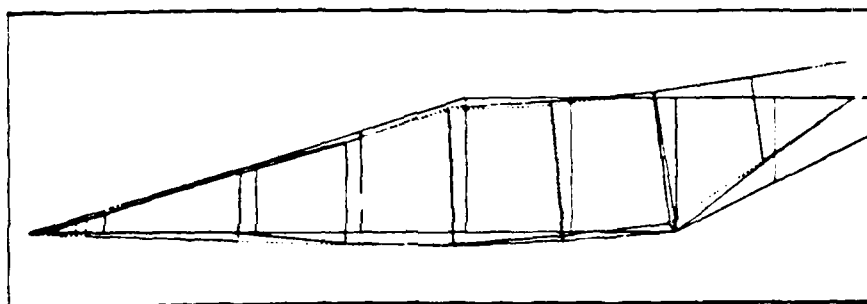
(1) Since both profiles were generated using the random number generator function, RANF, both are random profiles. Thus their contribution to Eqs. (33), i.e. the force input via Eq. (16) and (17) is random.

Each profile generates a different force input.

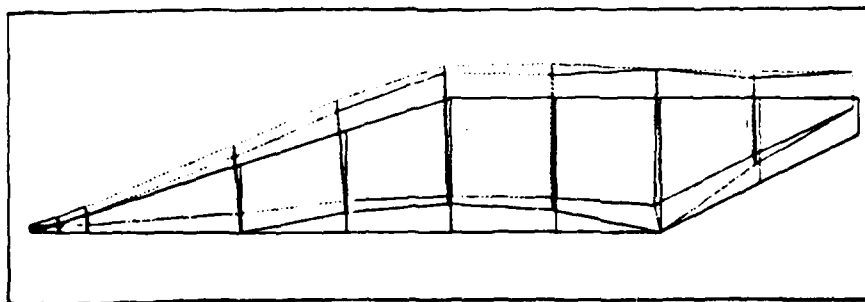
(2) Also the inertial loads were calculated separately at a different peak time for each slipper. As Tables 2a and 2b shown, for the same value of stiffness, the dynamic force is a maximum at different peak times for the same slipper. For example, for $k_A = k_F = 48 \times 10^4$, at slipper 1 the peak time for the original SLEDYNE profile is 1.416 sec. while the peak time for the Monte Carlo profile is 1.980.



$$\lambda_1 = 103$$

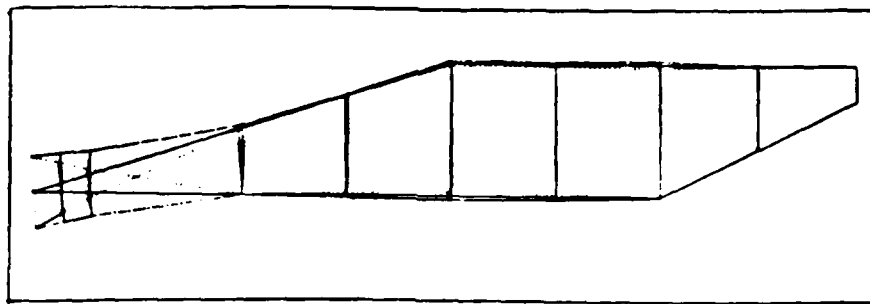


$$\lambda_2 = 123$$

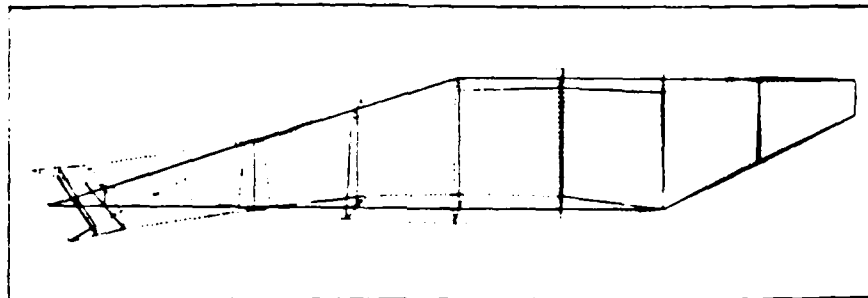


$$\lambda_3 = 156$$

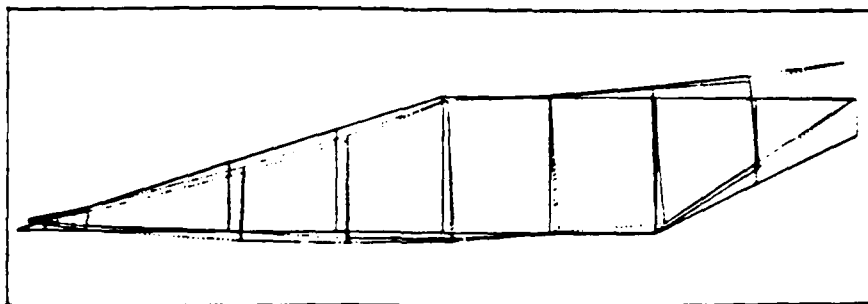
Figure 10. First Six Frequencies and Mode Shapes



$$\lambda_4 = 182$$



$$\lambda_5 = 185$$



$$\lambda_6 = 212$$

Figure 10. First Six Frequencies and Mode Shapes

MAXIMUM ACCELERATIONS IN IN/SEC²/10⁵

$k_A = k_F$ lbs/in	PEAK TIME	SLIPPER	\ddot{z}	$\ddot{\theta}$	\ddot{q}_1	\ddot{q}_2	\ddot{q}_3	\ddot{q}_4	\ddot{q}_5	\ddot{q}_6
48×10^4	1.416	AT 1 (F1)	.0933	.0030	-.4320	.1374	.0043	0.0	0.0	.1144
	.220	2 (F2)	.0521	.0027	-.3785	.1070	.0573			.2214
	1.455	3 (A1)	.1344	.0003	-.2229	.0084	-.1107			.0369
	.571	4 (A2)	-.0669	-.0033	.5553	-.1288	.0859			-.3554
96×10^4	.777	AT 1 (F1)	.4191	.0023	-.7905	.1523	-.4295	0.0	0.0	-.0298
	1.911	2 (F2)	-.0840	-.0047	.7249	-.2117	-.1578			-.2549
	1.420	3 (A1)	.5900	.0013	-1.1160	.2160	-.6894			-.1109
	.492	4 (A2)	.0976	-.0005	-.2868	.0831	-.0659			-.1310
192×10^4	.874	AT 1 (F1)	-.2859	-.0047	.9698	-.2039	.2856	0.0	0.0	-.4293
	.735	2 (F2)	-.4588	-.0015	.4576	-.1376	.5868			.0386
	1.455	3 (A1)	.1025	.0002	-.5282	.0425	.0366			.1264
	.492	4 (A2)	.3016	-.0057	.1931	-.0298	-.3212			-.5836

TABLE 2a. RESULTS OF ORIGINAL SLEDYNE PROFILE

MAXIMUM ACCELERATIONS IN IN/SEC²/10⁵

$k_A = k_F$ 1bs/in	PEAK TIME	SLIPPER	\ddot{z}	$\ddot{\theta}$	\ddot{q}_1	\ddot{q}_2	\ddot{q}_3	\ddot{q}_4	\ddot{q}_5	\ddot{q}_6
48×10^4	1.980	AT 1 (F1)	.4168	.0093	-1.9010	.4211	-.4088	0.0	0.0	.6356
	.917	2 (F2)	.0108	-.0031	.4285	-.0914	-.1065			-.1875
	.864	3 (A1)	.1506	-.0085	1.0660	-.2509	-.2977			-.6802
	1.148	4 (A2)	.6893	-.0093	.6759	-.1940	-1.1130			-.8457
96×10^4	1.625	AT 1 (F1)	-.9444	-.0033	1.7070	-.3728	1.1610	0.0	0.0	-.0406
	.535	2 (F2)	-1.2600	-.0071	2.5910	-.5049	1.4670			-.1178
	.884	3 (A1)	1.2120	-.0013	-1.2160	.2459	-1.6200			-.0803
	.061	4 (A2)	.8307	-.0174	1.7870	-.4389	-1.4420			-1.2890
192×10^4	1.625	AT 1 (F1)	-1.2640	-.0113	3.3110	-.7331	1.4020	0.0	0.0	-.6684
	.394	2 (F2)	-1.6260	-.0148	4.1500	-.8603	1.6620			-.4007
	.426	3 (A1)	.7412	-.0172	1.9320	-.4252	-1.2370			-1.4090
	1.765	4 (A2)	2.8470	-.0012	-3.1180	.5939	-3.7320			-.7058

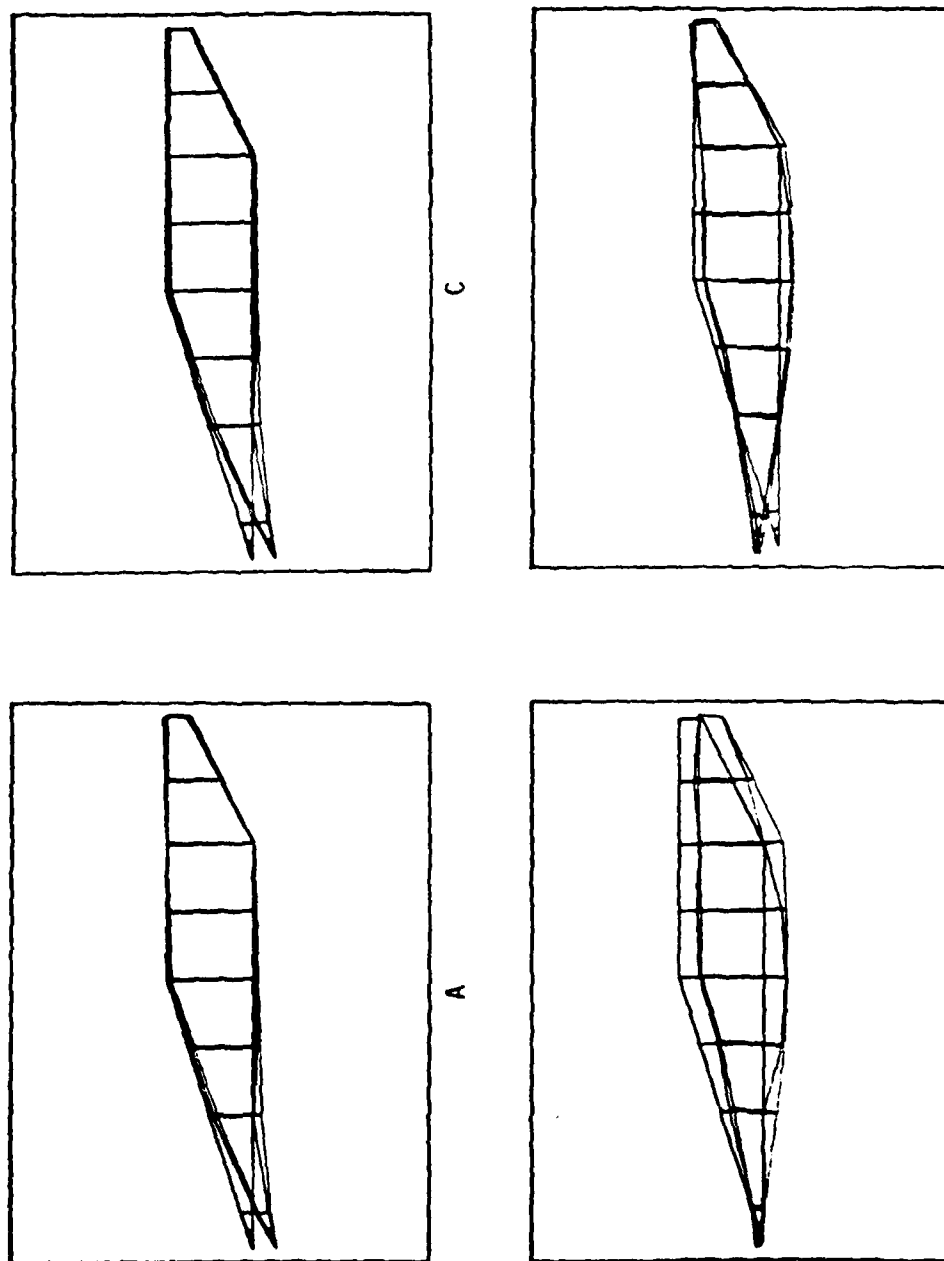
TABLE 2b. RESULTS OF MONTE CARLO PROFILE

$k_A = k_F$ lbs/in	TOTAL STRAIN ENERGY OF THE SLED IN IN-LB			
	PEAK AT FORWARD SLIPPER 1	PEAK AT FORWARD SLIPPER 2	PEAK AT AFT SLIPPER 1	PEAK AT AFT SLIPPER 2
48.0×10^4	78.267	57.791	22.676	42.927
96.0×10^4	62.444	188.610	133.541	150.834
192.0×10^4	63.057	220.456	397.554	488.070

TABLE 3a. RESULTS OF ORIGINAL SLEDYNE PROFILE

$k_A = k_F$ lbs/in	TOTAL STRAIN ENERGY OF THE SLED IN IN-LB			
	PEAK AT FORWARD SLIPPER 1	PEAK AT FORWARD SLIPPER 2	PEAK AT AFT SLIPPER 1	PEAK AT AFT SLIPPER 2
48.0×10^4	107.545	21.333	108.488	62.634
96.0×10^4	113.951	207.163	254.997	289.792
192.0×10^4	263.416	666.095	228.741	725.191

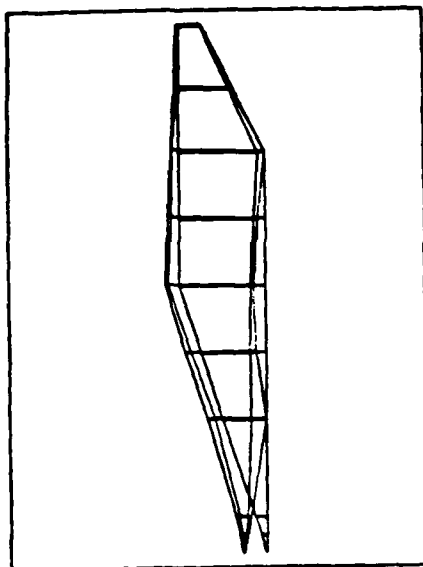
TABLE 3b. RESULTS OF MONTE CARLO PROFILE



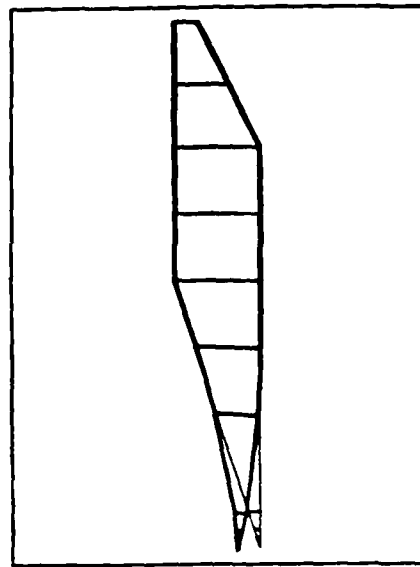
- A. PEAK FORCE AT FORWARD SLIPPER 1
 B. PEAK FORCE AT AFT SLIPPER 1
 C. PEAK FORCE AT FORWARD SLIPPER 2
 D. PEAK FORCE AT AFT SLIPPER 2

ORIGINAL SLEDYIE PROFILE
 $k_A = k_F = 48.0 \times 10^4$

Figure 11. Deformation Plots

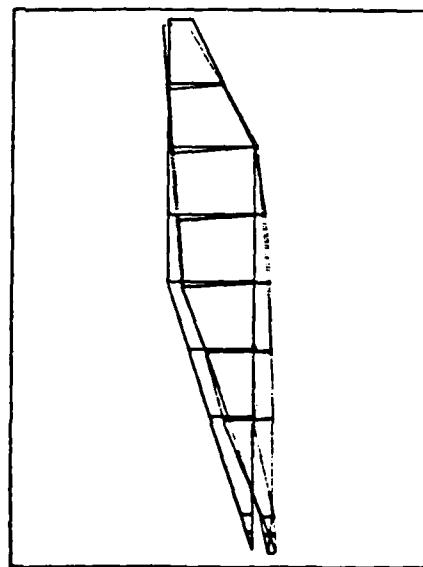


C

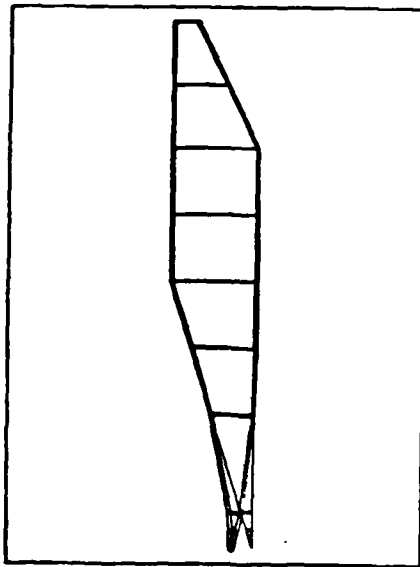


D

- A. PEAK FORCE AT FORWARD SLIPPER 1
- B. PEAK FORCE AT AFT SLIPPER 1
- C. PEAK FORCE AT FORWARD SLIPPER 2
- D. PEAK FORCE AT AFT SLIPPER 2



A

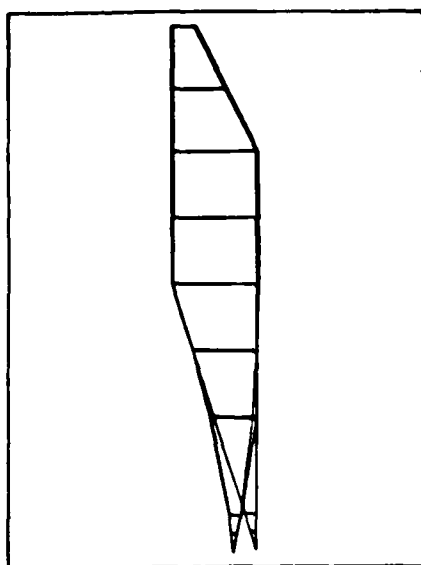


B

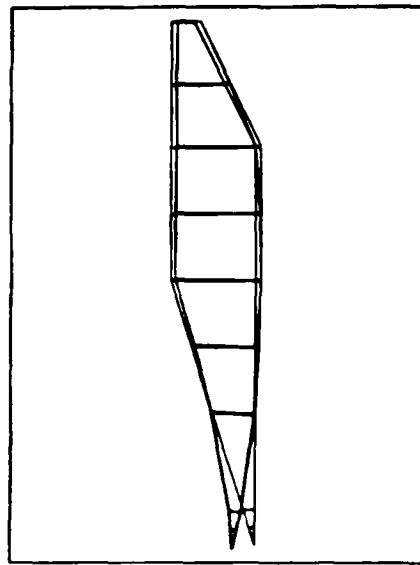
ORIGINAL SLEDYNE PROFILE

$$k_A = k_F = 96.0 \times 10^4$$

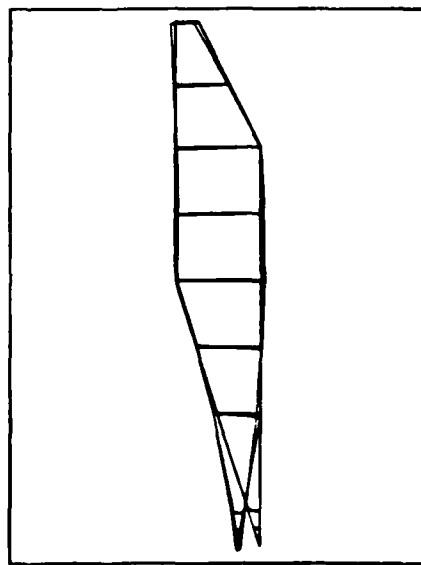
Figure 12. Deformation Plots



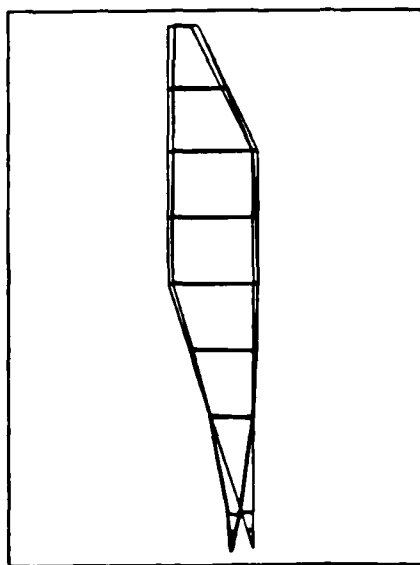
C



D



A



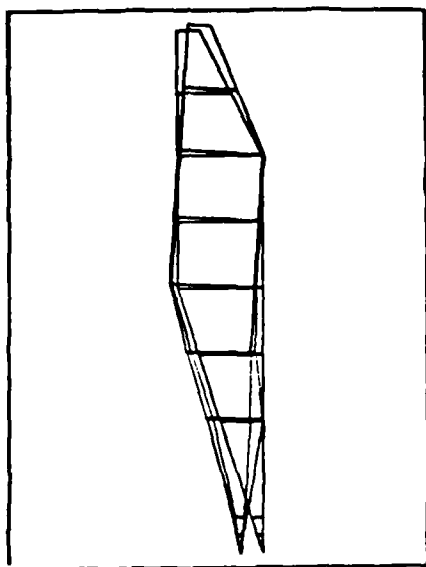
B

ORIGINAL SLEDYNE PROFILE

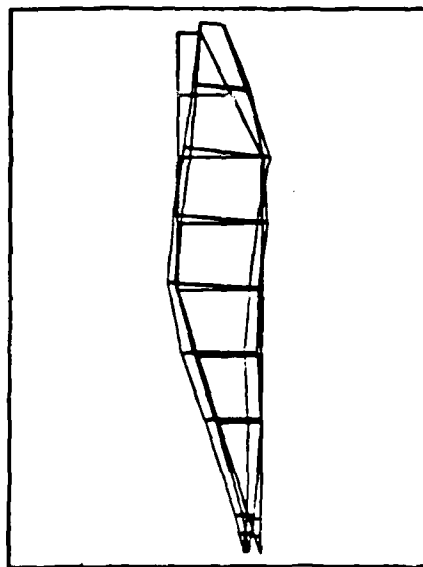
$$k_A = k_F = 192.0 \times 10^4$$

- A. PEAK FORCE AT FORWARD SLIPPER 1
- B. PEAK FORCE AT AFT SLIPPER 1
- C. PEAK FORCE AT FORWARD SLIPPER 2
- D. PEAK FORCE AT AFT SLIPPER 2

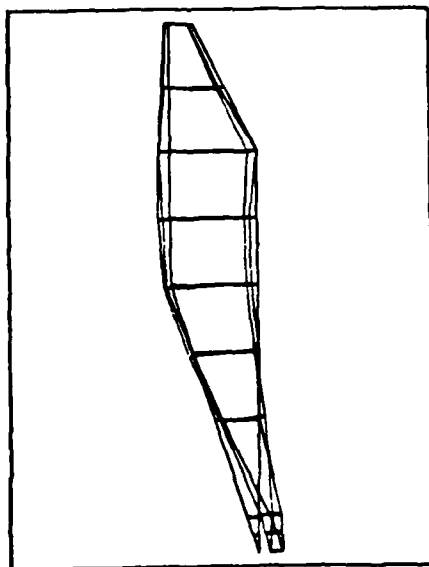
Figure 13. Deformation Plots



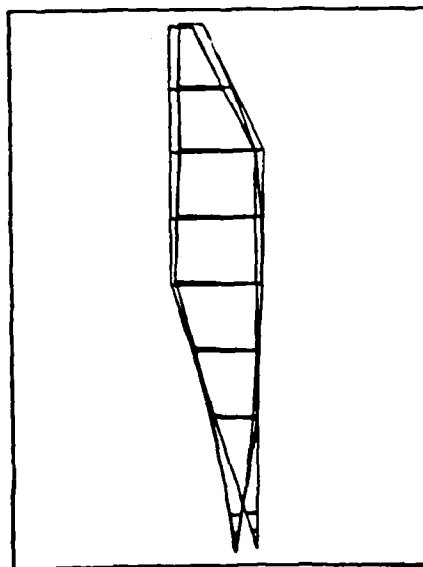
C



D



A

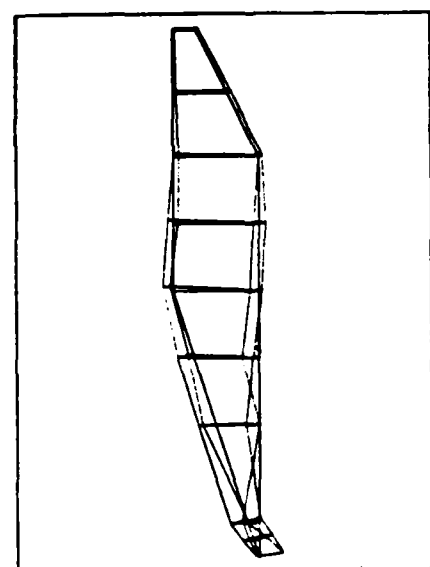


B

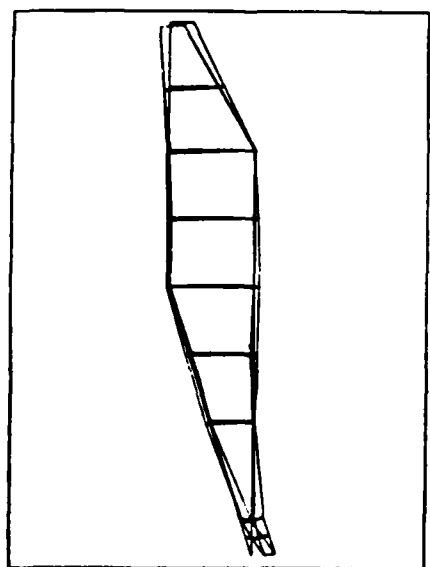
MONTE CARLO PROFILE
 $k_A = k_F = 48.0 \times 10^4$

A. PEAK FORCE AT FORWARD SLIPPER 1
 B. PEAK FORCE AT AFT SLIPPER 1
 C. PEAK FORCE AT FORWARD SLIPPER 2
 D. PEAK FORCE AT AFT SLIPPER 2

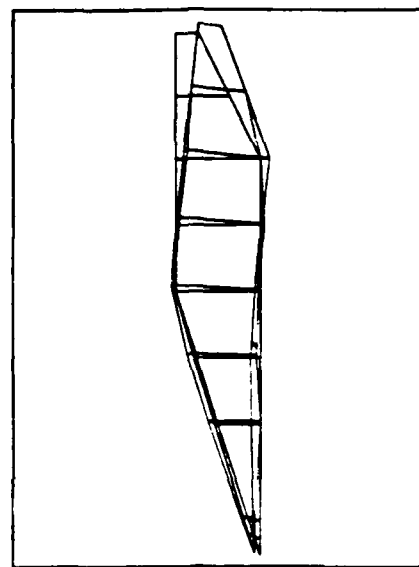
Figure 14. Deformation Plots



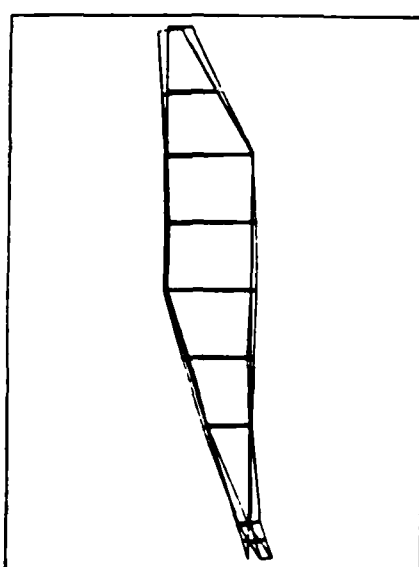
A



B



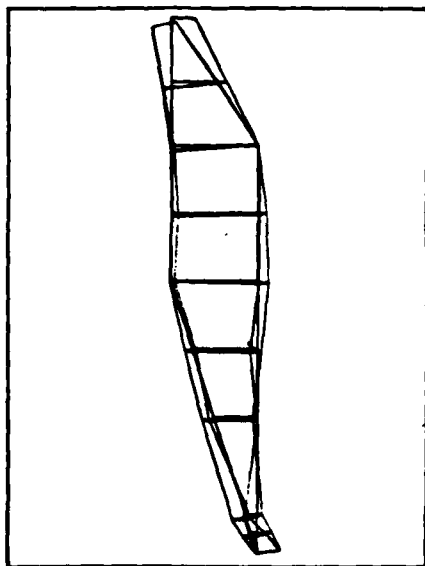
C



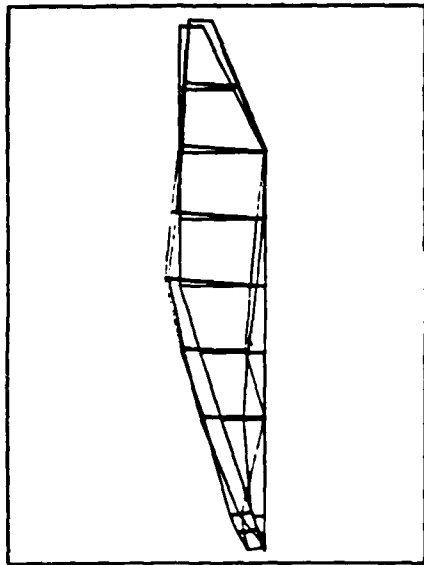
D

- MONTE CARLO PROFILE
 $k_A = k_F = 96.0 \times 10^4$
- A. PEAK FORCE AT FORWARD SLIPPER 1
 - B. PEAK FORCE AT AFT SLIPPER 1
 - C. PEAK FORCE AT FORWARD SLIPPER 2
 - D. PEAK FORCE AT AFT SLIPPER 2

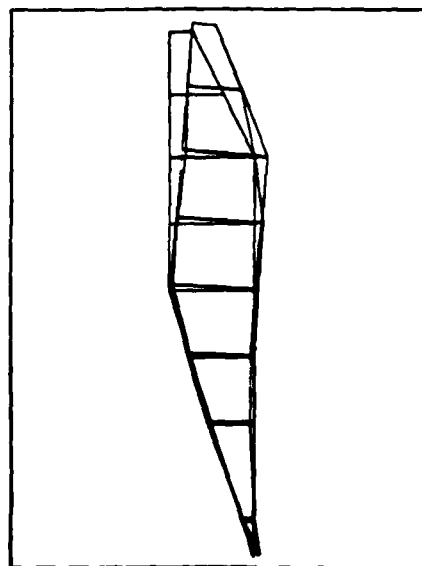
Figure 15. Deformation Plots



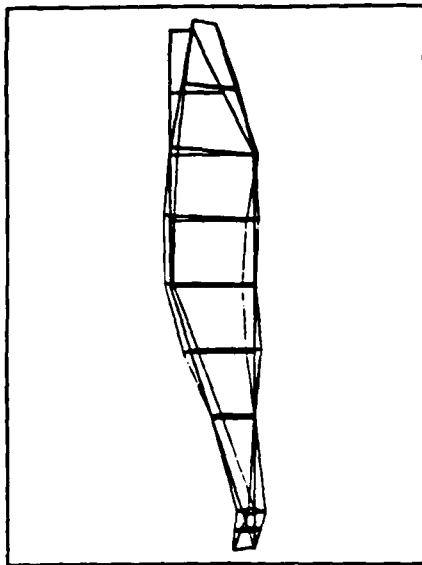
A



C



B



D

MONTE CARLO PROFILE
 $k_A = k_F = 192.0 \times 10^4$

A. PEAK FORCE AT FORWARD SLIPPER 1
 B. PEAK FORCE AT AFT SLIPPER 1
 C. PEAK FORCE AT FORWARD SLIPPER 2
 D. PEAK FORCE AT AFT SLIPPER 2

Figure 16. Deformation Plots

VI. CONCLUSIONS

The dynamics of a sled ride on rails at high speeds is an extremely complex phenomena. The factors that affect the ride are numerous and adequate simulation can only be achieved by extensive testing. The SLEDYNE program represents a preliminary attempt at introducing some sophistication to modeling stiffness/mass properties of the sled and the rail roughness profile. An extensive test program is necessary in order to validate the results obtained from analytical programs like SLEDYNE. For example there is no simplified way at present to determine the slipper stiffnesses k_A and k_F . Both the slipper beam assembly and the track flexibility affect these stiffnesses.

The aerodynamic data is even less sophisticated than the mass/stiffness properties. The extent of this deficiency cannot be assessed without parametric studies involving thrust, lift and drag. As in slipper stiffness data, no simple approach is presently available for determining the aerodynamic parameters.

However, some specific conclusions can be derived from this thesis.

(1) For example, the total strain energy of the sled increased in general as the values of slipper stiffness, $k_A = k_F$, increased for both profiles. However, exceptions can occur as was shown in Tables 3a and 3b.

(2) From the limited data obtained in our study, it would appear that the torsional rigidity in the sled structure is large enough to prevent dissimilar motion of opposite sets of slippers.

(3) Within a given profile, the effect of a variation in slipper stiffness could be more adequately measured, if the accelerations were available at the same time for a given slipper. Then, the total strain

energies could be compared for the resulting inertial loads.

(4) It wasn't possible to directly compare the results of the original SLEDYNE rail roughness profile (Tables 2a and 3a) and the Monte Carlo profile (Tables 2b and 3b), because the profiles were generated by a random function. In addition, for the original SLEDYNE case a separate profile was generated for each rail. It was felt that this did not satisfy the true physical phenomena that may occur. While, in the Monte Carlo case, a separate profile was generated for each slipper. So each profile generated a different force input in Eq. (40). However, by comparing Tables 2a and 2b one observes that the physical characteristics of the structure are quite similar. In particular, the bending stiffness produces a small amount of pitch acceleration, $\ddot{\theta}$. Yet the Monte Carlo profile on each slipper, in general, would have a larger $\ddot{\theta}$ as would be expected. In order to make a comparison within the Monte Carlo profile, a statistical approach must be made due to the individual slipper profile concept.

(5) For the user, the Monte Carlo profile is not only easier to implement in the SLEDYNE program but also easily expandable if additional measured data becomes available. Additional or finer intervals can be defined to adequately represent any range of track measurements. Since the Monte Carlo ranges along the 0-1 scale are constructed (See Table 1) independently of the SLEDYNE program, a virtually unlimited amount of track measurements can be considered in defining the profile. Thus, neither the efficiency nor the core memory requirements of SLEDYNE are affected by the amount of rail roughness measurements. On the other hand, since the original SLEDYNE profile is generated internally in SLEDYNE, core requirements for it will be increased as the number of track measurements increase. Also additional data on the sequence of the segments selected plus the total

number of point entries must be stored for both rails, since a different rail roughness profile is generated for each rail. Therefore, the original SLEDYNE profile is not as amenable to expansion as the Monte Carlo profile.

(6) Although only two basic parameters have been examined, it is possible for one to investigate additional individual parameters with the use of the combined SLEDYNE and NASTRAN programs. For example, it is possible to study a variation in the aerodynamic forces with the combined SLEDYNE and NASTRAN programs. The author feels that this joint application is an extremely useful design tool which can be incorporated into future hypersonic sled development.

REFERENCES

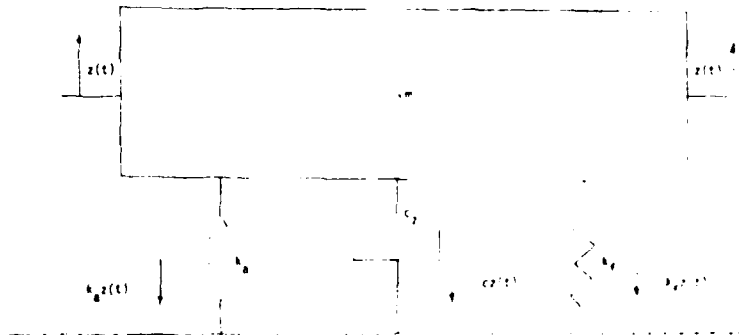
1. The Holloman Track - Facilities and Capabilities, Air Force Special Weapons Center, 6585th Test Group, Test Track Division, Holloman, AFB, New Mexico, 1974.
2. Istracon Handbook, Istracon Report No. 60-1, Interstation Supersonic Track Conference, Structures Working Group, Air Force Systems Command, Dec. 1961.
3. Dawson, K. L. and Kilner, J. R., Digital Computer Program for the Prediction of Taxi Induced Aircraft Dynamic Loads, Boeing Aerospace Co., April 1979.
4. Captain, K. M., Boghani, A. B. and Wormley, D. N., "Analytical Tire Models for Dynamic Vehicle Simulation", Vehicle System Dynamics 8, 1979, pp. 1-32.
5. Greenbaum, G. A., Garner, T. N., and Platus, D. L., Development of Sled Structural Design Procedures". AFSWC-TR-73-22, 6585th Test Group, Holloman, AFB, New Mexico, May 1973.
6. Meirovitch, L., Elements of Vibration Analysis, New York: McGraw-Hill Book Co., 1975.
7. Venkayya, V. B. and Cheng, F. Y., "Resizing of Frames Subjected to Ground Motion", International Symposium on Earthquake Structural Engineering, St. Louis, Missouri, August, 1976.
8. The Nastran Theoretical Manual (Level 17.0), NASA SP-221(04), National Aeronautics and Space Administration, Washington, D.C., Dec. 1977.
9. The Nastran User's Manual (Level 17.0), NASA SP-222(04), National Aeronautics and Space Administration, Washington, D.C., Dec. 1979.

10. Henrici, Peter, Discrete Variable Methods in Ordinary Differential Equations, New York: John Wiley & Sons, Inc., 1962.
11. Hildebrand, F. B., Introduction To Numerical Analysis, New York: McGraw-Hill Book Company, Inc., 1956.
12. Budnick, F. S., Mojena, R. and Vollman, T. E., Principles of Operations Research for Management, Illinois: Richard D. Irwin, Inc., 1977.
13. Kleijnen, J. P. C., Statistical Techniques in Simulation, Part 1, New York: Marcel Dekker, Inc., 1974.
14. Reitman, J., Computer Simulation Applications, New York: John Wiley and Sons, Inc., 1971.
15. Fisher, G. K. and Stronge, W. J., Analytical Investigation of Rocket Sled Vibrations Excited by Random Forces, U.S. Naval Ordnance Test Station, China Lake, California, NAVWEPS Report 8546, July 1964.
16. Plantema, F. F., Sandwich Construction, New York: John Wiley and Sons, Inc., 1966.
17. Allen, H. G., Analysis and Design of Structural Sandwich Panels, New York: Pergamon Press, 1969.
18. Venkayya, V. B. and Tischler, V. A., ANALYZE - Analysis of Aerospace Structures with Membrane Elements, AFFDL-TR-78-170, Flight Dynamics Laboratory, AFWAL/FIBR, Wright-Patterson AFB, Ohio, Aug. 1978.

APPENDIX A

This appendix provides the detailed steps required for the derivation of C_b , the damping coefficient at each slipper for bounce, Eq. (22), C_p , the damping coefficient at each slipper for pitch, Eq. (23), and damping coefficients C_F and C_A , Eq. (20) and (21).

To compute the damping coefficients associated with flexing of the stepper beam springs. For bounce, consider the following spring-mass-damper system.



Derive the equation of motion by taking the sum of the forces in the vertical direction

$$-k_F z - k_A z - C_z \dot{z} = m\ddot{z}$$

or

$$\ddot{z} + \frac{C_z}{m} \dot{z} + \frac{(k_A + k_F)}{m} z = 0 \quad (1A)$$

From Eq. (1A) the natural frequency ω_N is given by

$$\omega_N = \sqrt{\frac{(k_A + k_F)}{m}} \quad (2A)$$

Define $\omega_N = \omega_b$ where b implies bounce.

Also from Eq. (1A)

$$\frac{C_z}{m} = 2\xi_z \omega_b \quad (3A)$$

where ξ_z is the viscous damping factor.

Substituting Eq. (2A) into (3A) gives

$$C_z = 2\xi_z \left(\frac{(k_A + k_F)}{m} \right)^{1/2} m$$

or

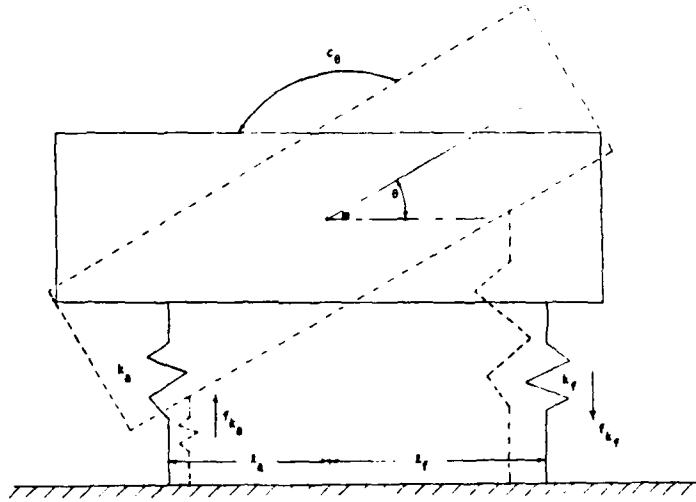
$$C_z = 2\xi_z \sqrt{(k_A + k_F)m} \quad (4A)$$

Thus the damping coefficient at each slipper for bounce is given by

$$C_b = \frac{C_z}{4} = \frac{1}{4} (2\xi_z \sqrt{(k_A + k_F)m}) \quad (5A)$$

Therefore Eq. (22) has been derived.

For pitch consider the following spring-mass-damper system.



where C_θ is a rotary damper. The forward slipper spring is being extended while the aft slipper spring is being compressed. For small values of θ ,

$$\begin{aligned} F_{k_F} &= k_F \ell_F \theta \\ F_{k_A} &= k_A \ell_A \theta \end{aligned} \quad (6A)$$

Derive the equation of motion by taking the sum of the moments about the cg.

$$-F_{k_F} \ell_F - F_{k_A} \ell_A - C_\theta \dot{\theta} = I \ddot{\theta}$$

or

$$I \ddot{\theta} + C_\theta \dot{\theta} + F_{k_F} \ell_F + F_{k_A} \ell_A = 0 \quad (7A)$$

Substituting Eq. (6A) into Eq. (7A) gives

$$I \ddot{\theta} + C_\theta \dot{\theta} + (k_F \ell_F^2 + k_A \ell_A^2) \theta = 0$$

Thus

$$\ddot{\theta} + \frac{C_\theta}{I} \dot{\theta} + \frac{(k_F \ell_F^2 + k_A \ell_A^2)}{I} \theta = 0 \quad (8A)$$

From Eq. (8A) the natural frequency ω_N is given by

$$\omega_N = \sqrt{\frac{(k_F \ell_F^2 + k_A \ell_A^2)}{I}} \quad (9A)$$

Define $\omega_N = \omega_\theta$ where θ implies pitch.

Also from Eq. (8A)

$$\frac{C_\theta}{I} = 2\xi_\theta \omega_\theta \quad (10A)$$

where ξ_θ is the viscous damping factor.

Substituting Eq. (9A) into Eq. (10A) gives

$$C_\theta = 2\xi_\theta \left(\sqrt{\frac{(k_F \ell_F^2 + k_A \ell_A^2)}{I}} \right) I$$

or

$$C_{\theta} = 2\xi_{\theta} \left(\sqrt{(k_F \ell_F^2 + k_A \ell_A^2) I} \right) \quad (11A)$$

Thus the damping coefficient at each slipper for pitch is given by

$$C_P = \frac{C_{\theta}}{2(\ell_F^2 + \ell_A^2)} = \frac{1}{2(\ell_F^2 + \ell_A^2)} \left(2\xi_{\theta} \sqrt{(k_F \ell_F^2 + k_A \ell_A^2) I} \right) \quad (12A)$$

Therefore Eq. (23) has been derived.

Assume that the damping is not equal at each slipper but is proportional to the beam stiffness. Thus for a forward slipper

$$C_F = (C_b + C_P) \frac{2k_F}{k_A + k_F} \quad (13A)$$

and for an aft slipper

$$C_A = (C_b + C_P) \frac{2k_A}{k_A + k_F} \quad (14A)$$

Thus Eqs. (20) and (21) have been derived. The recommended value for ξ_z and ξ_{θ} is .03, i.e. 3% critical damping.

VITA

Victoria A. Tischler was born on 25 November 1939 in Pittsburgh, Pa. She graduated from Divine Providence Academy in Pittsburgh, Pa. in 1957. She graduated from Carnegie Institute of Technology in 1962 with a Bachelor of Science Degree in Mathematics and from California State College at Long Beach in 1966 with a Master of Arts Degree in Mathematics. In 1966 she was employed by the Air Force Flight Dynamics Laboratory as a mathematician at Wright-Patterson Air Force Base. During her employment there, she was assigned to the Structures Division in the Analysis and Optimization Branch. In 1976 she enrolled in the Air Force Institute of Technology in the graduate Aeronautical Engineering Program.

Permanent Address:
4938 Sweetbitch Drive
Dayton, Ohio 45424

UNCLASSIFIED

SECURITY CLASSIFICATION OF THIS PAGE (When Data Entered)

REPORT DOCUMENTATION PAGE		READ INSTRUCTIONS BEFORE COMPLETING FORM
1. REPORT NUMBER AFIT/GAE/AA/80D-22	2. GOVT ACCESSION NO. AD A094736	3. RECIPIENT'S CATALOG NUMBER
4. TITLE (and Subtitle) A Parametric Study of Certain Forcing Functions Related to a Hypersonic Sled		5. TYPE OF REPORT & PERIOD COVERED M. S. Thesis
7. AUTHOR(s) Victoria A. Tischler		6. PERFORMING ORG. REPORT NUMBER
9. PERFORMING ORGANIZATION NAME AND ADDRESS Air Force Institute of Technology (AFIT/ENA) Wright-Patterson AFB, Ohio 45433		8. CONTRACT OR GRANT NUMBER(s)
11. CONTROLLING OFFICE NAME AND ADDRESS Air Force Wright Aeronautical Laboratories Flight Dynamics Laboratory Wright-Patterson AFB, Ohio 45433		10. PROGRAM ELEMENT, PROJECT, TASK AREA & WORK UNIT NUMBERS
14. MONITORING AGENCY NAME & ADDRESS (if different from Controlling Office)		12. REPORT DATE December 1980
		13. NUMBER OF PAGES
		15. SECURITY CLASS. (of this report) Unclassified
		15a. DECLASSIFICATION/DOWNGRADING SCHEDULE
16. DISTRIBUTION STATEMENT (of this Report) Approved for public release; distribution unlimited.		
17. DISTRIBUTION STATEMENT (of the abstract entered in Block 20, if different from Report)		
18. SUPPLEMENTARY NOTES Approved for public release; IAW AFR 190-17 Frederic C. Lynch, Major, USAF Director of Public Affairs 30 DEC 1980		
19. KEY WORDS (Continue on reverse side if necessary and identify by block number) Dynamic Analysis Slipper Stiffness Hypersonic Sled Integrated Sled Design Rail Roughness Forcing Function Lagrange Equation Total Strain Energy		
20. ABSTRACT (Continue on reverse side if necessary and identify by block number) The rail roughness profile and the slipper stiffnesses are the important factors in determining the forcing function in the dynamic analysis of high speed rocket sleds. A parametric study involving a variation in the rail roughness profile and the slipper stiffnesses was performed. This study was carried out by interfacing the NASTRAN structural analysis program and a program called SLEDYNE developed for Holloman AFB. Using NASTRAN a free vibration analysis of the elastic sled body was made in order to obtain the natural frequencies and mode shapes. SLEDYNE simulates the sled ride on the		

DD FORM 1 JAN 73 1473 EDITION OF 1 NOV 65 IS OBSOLETE

UNCLASSIFIED

SECURITY CLASSIFICATION OF THIS PAGE (When Data Entered)

UNCLASSIFIED

SECURITY CLASSIFICATION OF THIS PAGE(When Data Entered)

rails and computes a set of inertial forces acting on all the mass points of the sled. The response of the sled to this inertial loading was determined by a NASTRAN static analysis.

Two rail roughness profiles were considered, both based on the same set of track measurements, and three values of slipper stiffness were used. Response to the parametric study was measured by the total strain energy of the sled and the displacements of the mass points of the sled.

UNCLASSIFIED

SECURITY CLASSIFICATION OF THIS PAGE(When Data Entered)

UNCLASSIFIED

SECURITY CLASSIFICATION OF THIS PAGE (When Data Entered)

rails and computes a set of inertial loadings on all the mass points of the sled. The response of the sled to this inertial loading was determined by a NASTRAN static analysis.

Two rail roughness profiles were considered, both based on the same set of track measurements, and three values of slipper stiffness were used. Response to the parametric study was measured by the total strain energy of the sled and the displacements of the mass points of the sled.

UNCLASSIFIED

SECURITY CLASSIFICATION OF THIS PAGE (When Data Entered)

DATE
FILMED
— 8